Eulerian–Lagrangian spray atomization model coupled with interface capturing method for diesel injectors

J. Anez, Aqeel Ahmed, N. Hecht, B. Duret, Julien Reveillon, F.X. Demoulin

Eulerian-Lagrangian Spray Atomization model coupled with Interface Capturing Method for Diesel injectors

J. Anez, A. Ahmed, N. Hecht, B. Duret, J. Reveillon*, F.X. Demoulin

CORIA-UMR 6614 - Normandie University, CNRS-University and INSA of Rouen, 76800 Saint Etienne du Rouvray, France.

Abstract

Traditional Discrete Particle Methods (DPM) such as the Euler-Lagrange approaches for modeling atomization, even if widely used in technical literature, are not suitable in the near injector region. Indeed, the first step of atomization process is to separate the continuous liquid phase in a set of individual liquid parcels, the so-called primary break-up. Describing two-phase flow by DPM is to define a carrier phase and a discrete phase, hence they cannot be used for primary breakup. On the other hand, full scale simulations (direct simulation of the dynamic DNS, and interface capturing method ICM) are powerful numerical tools to study atomization, however, computational costs limit their application to academic cases for understanding and complementing partial experimental data. In an industrial environment, models that are computationally less demanding and still accurate enough are required to meet new challenges of fuel consumption and pollutant reduction. Application of DNS-ICM methods without fairly enough resolution to solve all length scales are currently used for industrial purposes. Nevertheless, effects of unresolved scales are generally cast aside. The Euler-Lagrange Spray Atomization model family (namely, ELSA, also called, $\Sigma - Y$ or $\Omega - Y$) developed by Vallet and Borghi pioneering work [1], and [2], at the contrary aims to model those unresolved scales. This approach is actually complementary to DNS-ICM method since the importance of the unresolved term depends directly on mesh resolution. For full interface

*Corresponding author : Julien.Reveillon@coria.fr

resolution, the unclosed terms are negligible, except in the far-field spray when the unresolved terms become dominant. Depending on the complexity of the flow and the available computational resources, a Large Eddy Simulation (LES) formalism could be employed as modeling approach. This work focus on the two main terms that drive these different modeling approaches namely the sub-grid turbulent liquid flux and the unresolved interface. Thanks to the open source library OpenFoam® [3] this work is an attempt to review and to release an adapted modeling strategy depending on the available mesh resolution. For validation, these solvers are tested against realistic experimental data to see the overall effect of each model proposal. It was found that both showed good agreement with experiments, and particularly under Diesel Spray injection conditions, the sub-grid scales represent the major driving force, thus diffusing the interface rapidly at the exit of the injector.

Keywords: Euler-Lagrange Spray Atomization model, ELSA, ICM, LES, atomization

1. Introduction

Several strategies can be found in literature to model fuel injection and to cope with the multi-phase / multi-scale nature of the flow. A full resolution of the interface thanks to direct numerical simulation (DNS), using either interface capturing methods or/and reconstruction methods [4, 5, 6, 7] is unfeasible as far as industrial applications are concerned, due to prohibitive computational costs.

In any event, an atomization process resulting in a spray, composed of spherical droplets surrounded by a gaseous environment, needs to be modeled with well established methods. Many approaches are based on kinetic theory, where the spray is described through a number density function that verifies the Williams-Boltzmann Equation (WBE) [8]. Physical processes such as particle transport, drag and phase change can be implemented in this formalism. A widely used

approach to solve the WBE is the Lagrangian-Monte-Carlo method [9], where the liquid is tracked with a Lagrangian description and the gas is solved in an Eulerian framework. Its interest lies in a straightforward implementation of physical processes such as evaporation and secondary break-up. However, the computational cost of such method remains important, especially in unsteady configurations. Indeed, an high number of stochastic particles (usually called parcels) is required in each cell of the numerical domain to obtain statistical convergence. Another approach to solve the WBE is to consider a Euler-Euler (EE) formalism, where both phases are treated as a continuum. This solution is very attractive to describe the evolution of the spray characteristics : the computation cost is moderate compared to Lagrangian approaches and parallelization is straightforward. These features are even more prevalent considering the growing use of Large Eddy Simulation (LES) to achieve a physical description of the gas flow field.

However, despite the efficiency of Eulerian methods on actual super-computers, the direct resolution of WBE is generally infeasible since the dimension of the problem is multiplied by the number of spray characteristics (position, velocity, size, temperature, etc) retained. This feature constrains these methods to address a limited description of these properties. The numerous possible hypotheses have led to an abundant research in this framework. For instance, in Multi-Fluids models [10, 11] the droplet geometry information is discretized in sections to represent the spray distribution. Another solution [12] is a smooth reconstruction based on a sum of kernel of the density functions and a quadrature method of moments employed for this purpose. Nevertheless, all these methods based on WBE assume generally that the spray is composed by numerous individual spherical droplets with well-defined features as position or diameter, which is far from being the case with atomizers generally employed in an industrial context. Indeed, the liquid phase is initially a continuum (i.e. liquid jet or film) and it is not possible to define such well-defined characteristics until the end of primary breakup. Therefore, a more general description of the

two-phase flow has been developed in this paper, following Vallet and Borghi [1] pioneering works.

In these models, the boundary separating pure liquid and pure gas is considered as a mixing zone. Meaning that both liquid and gas phases coexist at the same macroscopic position with an occupied portion of volume defined by the liquid volume fraction (α_l). In this context, two family of equilibrium models have been developed. A first possibility [13] is to use the liquid volume fraction as the unique variable allowing the description of the interface. Another set of approaches is based on a transport equation for the liquid/gas interface density [4, 1].

In this second group of models, the Eulerian-Lagrangian Spray Atomization (ELSA) model has been developed intensively during the last twenty years [4, 1]. From this work, different models based on Eulerian modeling for atomization have been studied. Later on, Blokkeel et al. [14] completed the original approach by a Lagrangian description of the spray once the primary break-up is achieved. In addition, they proposed to call this approach ELSA for Eulerian-Lagrangian Spray Atomization model to simplify its denomination, but other names are still in use such as, $\Sigma - Y$, $\Omega - Y$ or ESA, depending on which variable has been retained or whether the Lagrangian phase has been activated or not. Moreover, a new model has been attached to this approach such as Quasi-Multiphase Euler flow [15, 16] to account for slip velocity between phase. An extension to LES has been first carried out by Chesnel et al. [17]. All in all, they belong to the ELSA family models that try to consider and to model two main terms that drive atomization process for non-fully resolved cases: the subgrid/unresolved turbulent liquid flux $R_{\alpha i}$ and the unresolved liquid gas interface that will be characterized in this work by Σ' (liquid gas interface area per unit of volume).

The purpose of the present work is therefore to present a multi-scale approach suitable to perform LES of atomization together with the possibility to

recover ICM/DNS features for well resolved interface flow. To achieve this goal, the most important unresolved phenomena to address are the sub-grid turbulent liquid flux and surface density transport equation to which models based on ELSA concept are developed. The work is organized as follows: section 2 is devoted to the description of the Eulerian solver directly derived from ELSA formulation. Then, an innovative coupling between an Interface Capturing Method (ICM) and a complete ELSA approach is detailed. Section 3 accounts for the numerical configuration. Subsequently, section 4 reports the validation process of the proposed Eulerian solver in which different well-established turbulence models, such as $k-\varepsilon$ [18, 19], Smagorinksy [20, 21], WALE [22], and modeling strategy, namely, ELSA and ICM coupled with ELSA are compared against experimental data. Finally, in section 5 conclusions are sketched and the best numerical match with the experiments is presented.

2. Modeling Approach

Commonly, the term *multiphase flow* is used to refer any fluid flow consisting of more than one phase or component [23]. One could classify them according to the state of different phases or components (gas/solid flows, or liquid/solid flow or gas/particle flow or bubbly flow and so on). In the context of this article only two-phase flow is considered: a liquid phase and a gas phase separated by a well defined liquid-gas interface. Therefore, two topologies can be identified, namely *discrete flows* and *separated flows*.

Discrete flows consist of well defined particles distributed in a connected volume of continuous phase. There are two models prevalent in disperse flows, *trajectory models* and *two-fluid models* [23]. In the former, the motion of discrete phase is assessed by following either the motion of actual particles or the motion of stochastic particles (i.e. Parcels). Then, Lagrangian particle tracking can be used for small phase fractions. In the latter, *two-fluid models*, the discrete phase is treated as a second continuous phase on which conservation equations (of mass, momentum and energy) are developed for the two-fluid flow.

On the other hand, *separated flows* consists of two or more continuous streams of fluids separated by interfaces, thus interface capturing methods such as Volume of Fluid (VOF) [5, 24, 25] can be employed. Hybrid regimes, both discrete and separated flows, are formed when the interface between liquid and gas becomes deformed and droplets are generated, namely the atomization. For example, the breakup of a liquid jet propelled through a nozzle into a gaseous atmosphere (i.e. when the difference of velocity of this jet with respect to the surrounding gas is very strong and droplets are formed [1, 2]). In this case, it is not straightforward to define a discrete phase and a continuous phase as it is normally requested by multiphase flow approaches. Indeed, just at the exit of the injector nozzle, the amount of liquid phase is very high and this phase cannot be decomposed as sets of discrete particles. Moreover, bubbles could be present in the liquid flow due to penetration of the surrounding gas during the breakup process and to previous cavitation inside the nozzle injector. Consequently, the carrier phase would be the liquid and the discrete phase the gas bubbles. On the contrary, further downstream, a spray is created where the carrier phase is gas and the discrete phase corresponds to liquid droplets. Between these two limits, a two-phase flow exists with unclear discrete and carrier phases [4]. Once the flow is really a spray, disperse models such as Lagrangian approach should be used.

The key point of the proposed ELSA model is the analogy between atomization, liquid dispersion and turbulent mixing of a jet with large density difference with the ambient medium [1]. By using single-fluid approach, the choice of both carrier and discrete phases is avoided [4]. Therefore, the two-phase flow is studied as a single-fluid turbulent flow composed of two species with highly variable density. Note that the notion of two-phase flow still applies, in the sense that there are two velocities: one for the liquid and one for the gas that can be recovered thanks to the QME extension of ELSA approach [15, 16], which will be explained in little more detailed on the following pages.

2.1. Governing equations and modeling strategy

In this section, starting from this complete approach, for incompressible isothermal fluids governing equations are presented.

$$\begin{cases} \boldsymbol{\nabla} \cdot \boldsymbol{U} = 0 \quad , \\ \dfrac{\partial \rho \boldsymbol{U}}{\partial t} + \boldsymbol{\nabla} \cdot (\rho \boldsymbol{U} \otimes \boldsymbol{U}) = -\boldsymbol{\nabla} p + \boldsymbol{\nabla} \cdot (\rho \nu (\boldsymbol{\nabla} \boldsymbol{U} + \boldsymbol{\nabla} \boldsymbol{U}^t)) + \sigma \kappa \delta(\boldsymbol{x} - \boldsymbol{x}_s) \boldsymbol{n} + \rho \boldsymbol{f}_b \quad . \end{cases} \tag{1}$$

[1]

The continuity equation and the velocity $\boldsymbol{U}$ follow classical transport equations where p is the pressure, ν is the kinematic viscosity, $\sigma \kappa \delta(\boldsymbol{x} - \boldsymbol{x}_s)\boldsymbol{n}$ is the surface tension force applied at the liquid-gas interface position only, κ is the interface curvature, $\boldsymbol{x}_s$ is the interface position and $\boldsymbol{f}_b$ is the body forces per unit of mass. The dispersion of the liquid is described by a transport equation for the liquid volume fraction α_l, which represents the proportion of liquid in a given volume. For a chemically inert fluid, the equation writes:

$$\frac{\partial \alpha_l}{\partial t} + \boldsymbol{\nabla} \cdot (\boldsymbol{U} \alpha_l) = 0 \quad . \tag{2}$$

Solving these equations at all scales does not require any additional model and will be refereed as DNS. Nevertheless, these equations use generalized functions since the surface tension force occurs only at the surface and thus require a Dirac peak function representative of the interface $\delta(\boldsymbol{x} - \boldsymbol{x}_s)$. In addition the discontinuity of the liquid volume fraction entrains a discontinuity of density and viscosity, thus their derivatives also require generalized functions. To keep the interface sharp, the profile of the discontinuous variables across the interface, in particular the liquid volume fraction, has to remain a step profile. This expected feature has strong consequences on the numerical method for which dedicated interface capturing methods (ICM) are required for instance VOF

[1] density was added, to multiply the body force

[26], Level Set [27], Ghost-Fluid [28], among others. These ICM numerical approaches share a common feature, they are incompatible with a smooth profile of the liquid volume fraction, this point will be important later on.

Whenever it is not possible to solve these equations directly at all scales, some filtering or averaging process is applied that necessarily introduces new terms in the resulting two-phase equations. It is important to notice that one of the first feature that is lost is the accurate position of the interface. Previously, the liquid volume fraction field or any other phase indicator is sufficient to determine the position of the interface. For instance, any iso-surface of the liquid volume fraction in range [0,1] are identical if the liquid volume fraction profile is a step profile across the interface. But averaging or filtering will smooth the liquid volume fraction profile and let undetermined the actual position of the interface. Any other ICM faces the same problem but solves it in different ways. Either they force a sharp transition between liquid and gas at the interface which is in contradiction with the averaging/filtering procedure, or a smooth transition is considered with the consequence to loose the interface position. Notice that numerous successful works in the literature ignore these problems and used averaged/filtered approaches while keeping a sharp transition between phase. Meaning that RANS or LES approach are used and combined with ICM. It is expected that such effects are negligible if nearly all scales of the flow are resolved. The purpose of the present work is twofold :

- To consider and to propose models for unclosed terms issued from the averaging/filtering process
- To propose interface resolved quality (IRQ) sensors to evaluate when it is necessary to consider these models

Starting from the least resolved case where the two-phase flow considered is time-averaged (RANS approach), it is expected to recover the large-scales properties (penetration length and angle of dispersion of the liquid core) and small-scales characteristics (mean droplet diameter and their size distribution). Nevertheless, a large part of the flow has to be modeled, and models are then nec-

essarily dependent on the unresolved small scale features. The flows considered here are two-fluid flows with both characteristic Reynold and Weber numbers that tend to infinity [1]. In this case, early studies of liquid jets revealed that the turbulence was the primary initiator of break-up [29]. Subsequent studies, for instance [30, 31, 32, 33], have examined how this process works. In the early stages of breakup, the turbulent structures in the jet produce ligaments that are projected into the gaseous phase and then breaks to form droplets. All these phenomena lead to unresolved liquid dispersion that has to be represented by an appropriate model. Because the turbulence is the leading process for flows characterized by high Reynolds and Weber values, a kind of turbulent mixing has been considered initially [1]. This approach has given good results in many studies but can be augmented by accounting of particular liquid dispersion effect [34] or to include slipping motion between phases [15]. As a result, the velocity field in a two-phase flow and liquid volume fraction are studied in terms of mean and fluctuating values as for single-phase turbulent flows, based on the Reynolds decomposition [1].

The second approach is generally known as Large Eddy Simulation (LES) [17]. In order to separate different length scales in a turbulent flow field, a spatial filter is applied. Large scale structures that can be resolved by the numerical method on a given mesh are called the super-grid scales. The influence of all other (subgrid) scales to the super-grid behavior is modeled. The rationale behind this principle lies in the fact that the small scales of turbulence are more homogeneous and isotropic and therefore easier to model. As the mesh gets finer, the number of scales that require modeling becomes smaller, thus approaching the DNS [35]. But to recover truly the expected feature of the DNS in liquid-gas flows, ICM has to be activated since particular numerical models are necessary to represent the sharp interface transition.

2.2. Turbulence modeling

Before to go any further in the details of these RANS and LES approaches, both methods have to deal with density based correlations. There are two ways

to handle this problem, namely Reynolds or Favre averaging/filtering. Both approaches lead to modeling problems that are not yet completely solved. Using Reynolds averaging/filtering introduces correlation for which no models have been established yet for turbulent liquid-gas flow. Thus, these unclosed correlation are generally not considered or consider being part of Reynolds stress and turbulent liquid flux final model [15]. Regarding the Favre approach, it has been widely employed in single phase flow. However, as the density ratio increase, for instance in liquid-gas flow, the Favre averaging/filtering tends to over-conditioned the averaged variable based on the heavier phase. Numerically, it brings many problems of stability because of lack of information about the gas phase. In addition, Reynolds averaged/filtered velocity field is still *divergence free*, which is not the case for the Favre averaged/filtered velocity field. Despite these problems both Reynolds and Favre approaches have been applied successfully in the RANS context [2, 4, 36].

Here, Reynolds averaging/filtering formulation together with liquid volume fraction (volume formulation) field, instead of liquid mass fraction (mass formulation) is considered. This formulation is considered to be clearer by letting apparent the unclosed density correlation terms even if further efforts to define appropriate models still require future work. Applying the Reynolds averaging technique for incompressible flow to equations 1, and 2:

$$\begin{cases} \boldsymbol{\nabla} \cdot \bar{\boldsymbol{U}} = 0 \quad , \\ \dfrac{\partial \bar{\boldsymbol{\rho}} \bar{\boldsymbol{U}}}{\partial t} + \boldsymbol{\nabla} \cdot \left(\bar{\rho} \bar{\boldsymbol{U}} \otimes \bar{\boldsymbol{U}} \right) = -\boldsymbol{\nabla} \bar{p} + \boldsymbol{\nabla} \cdot \left(\overline{\rho \nu} (\boldsymbol{\nabla} \bar{\boldsymbol{U}} + \boldsymbol{\nabla} \bar{\boldsymbol{U}}^t) \right) + \bar{\rho} \bar{\boldsymbol{f}}_b - \boldsymbol{\nabla} \cdot \boldsymbol{R}_U + \tau_\rho \quad , \\ \dfrac{\partial \bar{\alpha}_l}{\partial t} + \boldsymbol{\nabla} \cdot (\bar{\boldsymbol{U}} \bar{\alpha}_l) = -\boldsymbol{\nabla} \cdot \boldsymbol{R}_{\alpha_l} \quad . \end{cases} \tag{3}$$

[2]

The term $\boldsymbol{R}_U$ is the so-called Reynolds stress tensor. The normal stresses

[2] averaged density was added, to multiply the body force

involve the respective variances of the x-, y- and z-velocity fluctuations. They are always non-zero because they contain squared velocity fluctuations. The shear stresses contain second moments associated with correlations between different velocity components [18]. The term on the RHS of the liquid volume fraction equation is the turbulent liquid flux, which will be studied in detail later. The mean mixture density reads: $\bar{\rho} = \rho_l \bar{\alpha_l} + \rho_g(1 - \bar{\alpha_l})$, with constant gas and liquid density, ρ_g and ρ_l, respectively.

To model these fluctuating terms, namely Reynolds stress tensor and the turbulent liquid flux, the Reynolds-Averaged NavierStokes (RANS) is firstly considered. Density correlations represented by τ_ρ appears on this Reynolds formalism. Their effect is still subject of research, e.g. density fluctuations in combustion processes are not necessarily applicable when the density ratio tends to infinity. Therefore, it will be considered as part of the global Reynolds stress model. It is clear that further work will be necessary to assess this hypothesis or to propose more appropriate models. Regarding the Reynolds stress, single-phase flow model is initially tested. Following Boussinesq's proposal, the turbulent momentum transport is assumed to be proportional to mean gradients of velocity [18]. By analogy, turbulent transport of a scalar is taken to be proportional to the gradient of the mean value of the transported quantity. Thus, the turbulent liquid flux is seen mainly as a dispersion term for the liquid due to a random turbulent motion. The formalism also shows that the turbulent liquid flux also contains the mean slip velocity of the liquid phase with respect to the mean mixture. The consideration of the slip velocity has been included

in recent works [15].

$$\begin{cases} \boldsymbol{R}_U & = (\overline{\overline{\boldsymbol{U}} \otimes \overline{\boldsymbol{U}}} - \bar{\boldsymbol{U}} \otimes \bar{\boldsymbol{U}}) \quad , \\ & \approx -\frac{\nu_t}{Sc_t}(\boldsymbol{\nabla}\bar{\boldsymbol{U}} + \boldsymbol{\nabla}\bar{\boldsymbol{U}}^t) \quad . \\ \boldsymbol{R}_{\alpha_l} & = (\overline{\overline{\boldsymbol{U}}\bar{\alpha_l}} - \bar{\boldsymbol{U}}\bar{\alpha_l}) \quad , \\ & = \bar{\alpha_l}(\bar{\boldsymbol{U}}|_{\boldsymbol{l}} - \bar{\boldsymbol{U}}) \quad , \\ & \approx -\frac{\nu_t}{Sc_t}\boldsymbol{\nabla}\bar{\alpha_l} \quad . \end{cases} \tag{4}$$

[3]

where ν_t is the turbulent viscosity (or sub-grid stress in LES framework) and Sc_t is the turbulent Schmidt number. On RHS of α_l equation 4, $\boldsymbol{R}_{\alpha_l}$ is the *turbulent liquid flux* that represents the transport of the liquid volume fraction induced by velocity fluctuations and is related to the unresolved part of the velocity that is known to produce additional dispersion. This formulation is only valid in the absence of slip velocity between phases. Indeed, if both phases are strictly non-miscible, it is possible to consider a so-called second order definition for the turbulent liquid flux:

$$\boldsymbol{R}_{\alpha_l} = \overline{\boldsymbol{u'}\boldsymbol{\alpha_l'}} = \bar{\alpha_l}(\bar{\boldsymbol{U}}|_{\boldsymbol{l}} - \bar{\boldsymbol{U}}) = \alpha_l\,(1-\alpha_l)\,\bar{\boldsymbol{V}}_{rlg} \quad . \tag{5}$$

This shows the strong link between $\boldsymbol{R}_{\alpha_l}$ and the local relative velocity $\boldsymbol{V}_{rlg}$ [34], that can be re-arranged as follows:

$$\bar{\boldsymbol{V}}_{rlg} = \left(\bar{\boldsymbol{U}}_l - \bar{\boldsymbol{U}}_g - \bar{\boldsymbol{V}}_D\right) = \left(\bar{\boldsymbol{U}}_{slg} - \bar{\boldsymbol{V}}_{Dlg}\right) \quad . \tag{6}$$

where $\bar{\boldsymbol{U}}_{slg}$ is the average relative velocity between the particle and the surrounding flow, and $\bar{\boldsymbol{V}}_{Dlg}$ is the drift velocity. In the case where the spray dynamic relaxation time τ_p and the mean effective slip velocity $\bar{\boldsymbol{U}}_{slg}$ are negligible (i.e., in the case of droplets with small Stokes numbers), the turbulent liquid flux is only

[3] here, 'equivalence' sign was added, in place of 'equality' sign

due to the drift velocity. Therefore, we will stick with the first order formulation presented in equation (4) which, based on the actual validation test case [37], was also proven to be successful. The interested reader might be then referred to [15] where this second order closure is further developed. Additionally, it has been proven [4, 15, 16] that even with this single flow approach it is possible to recover the different mean liquid and gas velocities $\bar{\boldsymbol{U}}|_{\boldsymbol{l}}$, and $\bar{\boldsymbol{U}}|_{\boldsymbol{g}}$, respectively by means of a drift flux model.

2.3. Turbulence models

Now the kinematic turbulent viscosity, ν_t, needs to be addressed. The accuracy of different RANS turbulence models when they are applied to turbulent two phase flows was studied previously [34]. It was shown that the **standard $k-\varepsilon$ turbulence model** (Launder and Spalding, 1974) is able to reproduce the main characteristics of two-phase flow if special care is devoted to the modeling of the turbulent mass flux. Nevertheless, the assumption of RANS models is that the turbulent viscosity, ν_t is isotropic: in other words, the ratio between Reynolds stress and mean rate of deformation is the same in all directions. Which is not the case within the scale spectrum of eddies. For instance, the smallest eddies are nearly isotropic and have a universal behavior. On the other hand, the largest eddies, which interact by extracting energy from the mean flow, are more anisotropic and their behavior is dictated by the geometry of the problem domain, the boundary conditions and body forces [18].

Another drawback of RANS models is the lack of generality in the "fitting-constant values", such as, C_μ, $C_{1\varepsilon}$, $C_{2\varepsilon}$, among others, when employed in axisymmetric jets cases [38]. Changing $C_{1\varepsilon}$ to 1.6 to fit the experimental data was proven to be effective [39] by increasing the rate of production of the kinetic energy. Pope [40] on the same line of research proposed a modified dissipation equation adapted to the round jet's lower spreading rate based on physical explanation. However, this modification was not validated for three-dimensional flows.

2.3.1. Large Eddies Simulation filtering

Instead of time-averaging, LES uses a spatial filtering operation to separate the largest and smallest eddies. Even though this simple approach permits to deal with flow anisotropy on large scales, which clearly is an advantage over RANS models, there are still some generality issues depending on the rate-controlling process [40]. However, in free shear flows at high Reynolds number, the transport process of interest are affected by the resolved large scales, which makes LES suitable for our case study. The method starts with the selection of a filtering function and a certain cutoff width with the aim of resolving in an unsteady flow computation all eddies with a length scale greater than the cutoff width. There are three well-known filtering functions, namely, *Top-hat filter*, *Gaussian filter* and *Spectral cutoff*. The first one is widely used in finite volume implementation. Further details can be found in [18]. The cutoff width is intended as an indicative measure of the size of eddies that are retained in the computations and the eddies that are rejected. In principle, we can choose the cutoff width Δ to be of any size, but in CFD computations with the finite volume method it is pointless to select a cutoff width that is smaller than the grid size. The most common selection is to take the cutoff width to be of the same order as the grid size, for instance, the cubic root of the grid cell volume:

$$\Delta = \sqrt[3]{\Delta x \Delta y \Delta z} \tag{7}$$

As before, starting from the Navier-Stokes and the liquid volume fraction equations, namely equations 1 and 2, respectively, LES-filtered continuity, momentum, and liquid volume fraction equations of the mixture yield:

$$\begin{cases} \boldsymbol{\nabla} \cdot \bar{\boldsymbol{U}} = 0 \quad , \\ \dfrac{\partial \bar{\boldsymbol{\rho}} \bar{\boldsymbol{U}}}{\partial t} + \boldsymbol{\nabla} \cdot \left(\bar{\rho} \bar{\boldsymbol{U}} \otimes \bar{\boldsymbol{U}} \right) = -\boldsymbol{\nabla} \bar{p} + \boldsymbol{\nabla} \cdot (\overline{\rho \nu} (\boldsymbol{\nabla} \bar{\boldsymbol{U}} + \boldsymbol{\nabla} \bar{\boldsymbol{U}}^t)) + \bar{\boldsymbol{f}}_b + \tau_\rho - \boldsymbol{\nabla} \cdot \boldsymbol{\tau}_u \quad , \\ \dfrac{\partial \bar{\alpha}_l}{\partial t} + \boldsymbol{\nabla} \cdot (\bar{\boldsymbol{U}} \bar{\alpha}_l) = -\boldsymbol{\nabla} \cdot \boldsymbol{\tau}_{\alpha_l} \quad . \end{cases} \tag{8}$$

Equations 8 should be solved to yield the filtered mixture velocity $\bar{\boldsymbol{U}}$, the filtered mixture pressure field $\bar{p}$, filtered mixture density $\bar{\rho} = \rho_l \bar{\alpha_l} + \rho_g(1 - \bar{\alpha_l})$, and the filtered liquid volume fraction distribution $\bar{\alpha_l}$. The last term on RHS results from the LES filtering operation, just like the Reynolds Stress, in this case commonly named the subgrid scale stress or **LES SGS**. However, unlike the Reynolds stresses in the RANS equations, the LES SGS stresses contain further contributions. Based on the flow variable decomposition $\phi(\mathbf{x}, t)$ as the sum of the filtered function $\bar{\phi}(\mathbf{x}, t)$ and $\phi^{'}(\mathbf{x}, t)$, which contains unresolved spatial variations. Now the SGS stresses can be written in the following form:

$$\boldsymbol{\tau}_u = (\bar{\rho}\overline{\boldsymbol{U}\boldsymbol{U}} - \bar{\rho}\bar{\boldsymbol{U}}\bar{\boldsymbol{U}}) = \underbrace{\bar{\rho}\overline{\bar{\boldsymbol{U}}\bar{\boldsymbol{U}}} - \bar{\rho}\bar{\boldsymbol{U}}\bar{\boldsymbol{U}}}_{Leonard} + \underbrace{\bar{\rho}\overline{\bar{\boldsymbol{U}}\boldsymbol{U}^{'}} + \bar{\rho}\overline{\boldsymbol{U}^{'}\bar{\boldsymbol{U}}}}_{cross} + \underbrace{\bar{\rho}\overline{\boldsymbol{U}^{'}\boldsymbol{U}^{'}}}_{LES} \quad . \tag{9}$$

The Leonard stresses are solely due to effects at resolved scales. The cross-stresses are due to interactions between the SGS eddies and the resolved flow. Finally, LES stresses are caused by convective momentum transfer due to interactions of SGS eddies and are modeled with SGS models explained in the following sections. For a complete definition and mathematical deduction see [18].

2.3.2. SGS Models

In order to the dynamics of the resolved scales to remain correct, the subgrid terms have to be modeled, i.e. the subgrid energy interaction with the resolved scales have to be reflected. In gas kinetics theory, molecular agitation draws energy from the flow by way of molecular viscosity. So the energy cascade mechanism [19] will be modeled by a term having a mathematical structure similar to that of molecular diffusion, but in which the molecular viscosity in (4) is replaced by a sub-grid viscosity ν_{sgs}. Mainly, two approaches were studied depending on the validation test case:

- *Models based on the resolved scales:* The subgrid viscosity is evaluated using global quantities related to the resolved scales. Within this category is

the well-known **Smagorinsky model**. Based on the assumption that the smallest turbulent eddies are almost isotropic, the Boussinesq approach is employed [20]. Thus, local SGS stresses τ, are taken to be proportional to the local rate of strain of the resolved flow [18]. The model is expressed, where C_{sgs} is constant and $|\bar{\boldsymbol{S}}|$ is the average strain rate of the resolved flow:

$$\nu_{sgs} = (C_{sgs}\Delta)^2 |\bar{\boldsymbol{S}}| \tag{10}$$

There are many authors that experimentally or numerically have demonstrated different values of the constant C_{sgs}, which makes the model flow-dependent. This gave an indication that the behavior of the small eddies is not as universal as was thought. Furthermore, the modeling requires a case-by-case adjustment or a more sophisticated approach.

- *Wall Adopting Local Eddy Viscosity (WALE) Model:* For reasons connected with the wall behavior of the subgrid-scale model, a new operator based on the traceless symmetric part of the square of the velocity gradient tensor S_{ij}^d is used. Consequently, the subgrid scale viscosity is modeled as [21] :

$$\nu_{sgs} = (C_w\Delta)^2 \frac{\left(S_{ij}^d S_{ij}^d\right)^{3/2}}{\left(\left(\bar{S}_{ij}\bar{S}_{ij}\right)^{5/2} + \left(S_{ij}^d S_{ij}^d\right)^{5/4}} \tag{11}$$

where C_w is a model constant and $\bar{S}_{ij}$ is the resolved-scale strain rate tensor. As reported in [22] WALE model shows better results in predicting near wall turbulence for wall bounded flows. No wall damping is necessary near wall regions in WALE model. Another study in channel separated flow performed by [41] shows that best match with DNS can be obtained using WALE model along-with power law wall function proposed by Werner and Wengle [42].

2.4. LES formulation compatible with ICM

An expected feature of LES model is to retrieve DNS (here ICM) characteristics for proper mesh resolution (tending to kolmogorov / Taylor length scales), i.e. for highly resolved flow, LES should switch from ELSA to ICM. In the following part, considering the known shortcomings of diffusive interfaces approaches in the dense spray region and in order to develop a model suitable also in the dilute spray region, a coupling technique between ELSA and an interface capturing method (ICM) is proposed. Firstly, F_σ is the additional force in the momentum equation due to the surface tension depending on the local curvature of the interface and is defined in equation 1 as $\sigma\kappa\delta(\boldsymbol{x}-\boldsymbol{x}_s)\boldsymbol{n}$. To compute this force and to apply the jump of any variable, the most accurate ICM-DNS code applies direct numerical schemes based on interface reconstruction, along with the numerical mesh characteristics. For instance, the ARCHER code [5] is based on coupled VOF-Level set method for interface reconstruction together with a ghost-fluid approach to represent accurately the discontinuity of variables such as density, pressure and viscosity at the interface. This reconstruction process generally depends on the mesh geometry, hence body-fitted methods based on unstructured mesh are used to address complex geometries. Notice that several proposals exist, for example in the open source software: OpenFOAM® to improve this point in particular the isoAdvector approach [43]. There are many successful examples in the literature of these fully resolved approaches combining ICM method with DNS using mesh resolution high enough to compute all the flow scales, based on the curvature, VOF-PLIC (piecewise-linear interface construction), VOF/level-set coupling for unstructured and non-uniform meshes, octree meshes, among others [44, 45, 46].

For full-scale resolution, ICM method aims at keeping a sharp interface, thus a discontinuous profile across the phases exits in particular during the convection process. This property is either directly included in the numerical scheme (VOF, Level-Set, ghost-fluid, among others) or obtained by additional correction designed to prevent numerical diffusion that could smear the profile.

The `interFoam` solver of OpenFOAM® is based on this last technique, where Weller [24] proposed to use an additional flux of liquid directed toward the interface proportional to the local velocity magnitude ($\boldsymbol{U}_r$) and located only where a mixture of liquid and gas exists (i.e. $\alpha_l \in [0,1]$), in such a way that the local flow steepens the gradient of the volume fraction and thus the interface resolution is improved [25]. This method is often referred as the VOF method, even if there is no real reconstruction of the interface. When using Direct Numerical Simulations (DNS), all fluctuations scales are solved up to the grid level and no averaged filtering is required. Consequently, the last term on the left-hand side in equation (12) will be equal to zero. On the other hand, following the modeling approach in this study, LES filtering or averaged under RANS framework is used. As for instance, diffusive methods are designed to smear the interface over several mesh cells to recover a continuous behavior of any variable. It is important to emphasize that the drift/slip behavior of the unresolved liquid flux is not compatible with the ICM method since the latter assumes the profile to be discontinuous. Hence, starting from the system reported in Equation. (8), the liquid volume fraction equation has been modified considering C_α as a pondering parameter between ELSA-base and an ICM approach.

$$\frac{\partial \bar{\alpha}_l}{\partial t} + \boldsymbol{\nabla} \cdot (\bar{\boldsymbol{U}} \bar{\alpha}_l) + \underbrace{\boldsymbol{\nabla} \cdot C_\alpha \boldsymbol{U}_r \bar{\alpha}_l (1 - \bar{\alpha}_l)}_{ICM} = \underbrace{(1 - C_\alpha) \boldsymbol{\nabla} \cdot (\boldsymbol{R}_{\alpha_l})}_{Elsa} \quad , \tag{12}$$

where

$$U_r = |\bar{U}| \frac{\nabla \bar{\alpha}_l}{|\nabla \bar{\alpha}_l|} \quad . \tag{13}$$

The advantages of the proposed solver is to determine a resolution of the interface with ICM in a limited region, whereas it is disabled when $\boldsymbol{R}_{\alpha_l}$ prevails (i.e. when the interface fluctuations become significant at subgrid-scale for instance in LES framework). An additional term is also added to the momentum equations 8 to account for the surface tension only when the interface is resolved, $C_\alpha F_\sigma$. The switching strategy is introduced through C_α and two different cri-

teria, based on the interface resolution and the curvature of the interface, have been proposed to determine its value. C_α was set zero (0) when the interface is poorly-resolved (dilute region) and set to one (1) otherwise (dense region).

430

- *First criteria:* IRQ_Σ. This criteria is given by the ratio of the minimum (resolved) interface area, Σ_{min}, over the actual interface area, Σ (eqn. 14). The interface area is more properly defined as "surface area of the liquid-gas interface per unit of volume", defined here as *liquid gas interface density*. And Σ_{min} corresponds to the minimum surface density that can be evaluated for a given value of resolved liquid volume fraction, where "a" is a length scale related to the control volume. In the framework of filtering by LES, this length is equal to the filter length scale. Here, a simple approach is used to evaluate Σ_{min}, however, if interface reconstruction was available, the actual resolved interface could be used. Σ follows an additional balance equation explained in the next section. Thus, the higher the surface interface fluctuates within a cell, the lower IRQ_Σ, which means subgrid effects become important.

$$\begin{cases} a\Sigma_{min} = 2.4\sqrt{\alpha_l(1-\alpha_l)} \quad , \\ IRQ_\Sigma = \dfrac{\Sigma_{min}}{\Sigma} \quad . \end{cases} \tag{14}$$

- *Second criteria:* IRQ_K. A grid-dependent parameter, especially if LES turbulence modeling is applied using as a cutoff width Δ, *cubic root of the grid cell volume*, defined in equation 7 [47]. Additionally IRQ_K takes into account the curvature of the interface, K, defined below. The less the interface curvature, the better resolution of the interface, thus C_α is then set to unity.

$$\begin{cases} K = \boldsymbol{\nabla} \cdot \left(\dfrac{\nabla \bar{\alpha}_l}{|\nabla \bar{\alpha}_l|} \right) \quad , \\ IRQ_K = \dfrac{1}{\Delta.K} \quad . \end{cases} \tag{15}$$

This model is thus able to take advantage of a full-interface resolution to recover a DNS formulation with ICM and to switch to a sub-grid approach when necessary. Note that ICM is not compatible with diffusive models, hence C_α will be dynamically adjusted to one or zero depending on the interface resolution within the cell. Furthermore, when the spray is formed and diluted, it is more accurate to use a regular method dedicated to solved the Williams-Boltzmann Equation (WBE) [8] and therefore a Lagrangian formulation is initiated.

2.5. Liquid Gas Interface Density Equation

So far the large-scales properties of two-phase flows have been defined by means of a balance equation of the liquid volume fraction, α_l. Now, the small-scale characteristics such as droplet size distribution and mean droplet diameter can be calculated by means of the *liquid gas interface density*, and Σ, which represents the liquid/gas surface interface per unit of volume. The concept of interface density is more general than droplet diameter or Sauter Mean Diameter (SMD). Indeed, liquid shapes are not always spherical and SMD cannot account for all other ligaments. Thus, Σ is a more generalized quantity able to quantify any type of interface. A closed form of Σ equation is not fully established yet. Starting with a phenomenological approach, as also presented by [2] and [4], a general filtered form may be written, following the same filtering procedure explained above:

$$\frac{\partial \bar{\Sigma}}{\partial t} + \boldsymbol{\nabla} \cdot (\bar{\boldsymbol{U}} \bar{\Sigma}) = \boldsymbol{\nabla} \cdot [\bar{\Sigma}(\bar{\boldsymbol{U}} - \bar{\boldsymbol{U}}_\Sigma)] + S_\Sigma \tag{16}$$

The first term of the right-hand side is unclosed since the interface velocity, $\bar{\boldsymbol{U}}_\Sigma$, is unknown. This term represents the difference between the interface velocity and the global mixture. It accounts for the dispersion of the interface by turbulence. Thus, namely, a first order closure (or gradient closure), as the aforementioned Boussinesq approximation, on which it is modeled as turbulent dispersion [4, 2], and neglecting any contribution of slip velocity, leads to the

following formulation:

$$\bar{\Sigma}(\bar{\boldsymbol{U}} - \bar{\boldsymbol{U}}_{\Sigma}) = \boldsymbol{R}_{\Sigma} = \frac{\nu_t}{Sc_t}\boldsymbol{\nabla}\bar{\Sigma} \tag{17}$$

The equation 16 for Σ takes into account two source terms included in S_{Σ}: firstly, the minimum production of the liquid-gas interface density induced by liquid-gas mixture and secondly, the production/destruction of liquid-gas interface density due to turbulent flow, vaporization, collision, and any coalescence in the dense part of the spray. Hence, the following equation arises:

$$S_{\Sigma} = \Sigma_{mix} + \Sigma_{int} \quad , \tag{18}$$

where Σ_{mix} refers to production of surface density due to liquid/gas mixing, and Σ_{int} represents production/destruction of surface density by the mean shear, turbulence and liquid structure interactions in this case. Vaporization is not considered in this work so far, however, Σ_{mix} is the necessary term that ensures the presence of interface simply because of co-existing phases. Vallet et al. [2] propose a formulation based on the inverse of the size of the control volume near the injector tip assuming a flat interface at the boundary. Lebas et al. [4] proposed that liquid characteristic scales are related to turbulent integral scale. In both cases, it is an initialization term that does not have a strong effect on the whole calculation, while producing a minimum surface density immediately after injection. The presence of an interface as long as the liquid comes into contact with the gas provide a mean to use a formulation based on minimum estimate of the surface density Σ_{min}, thus an additional quantity Σ' such that:

$$\Sigma = \Sigma_{min} + \Sigma' \tag{19}$$

Based on the assumption that surface density is at least equal to Σ_{min}, which is defined as the minimum amount of surface present due to liquid-gas mixing. Note that this definition is coupled with the amount of interface that can be obtained with ICM approach. As a result, it is required only to compute the

evolution of Σ'. Its transport equation is written as:

$$\frac{\partial \bar{\Sigma}'}{\partial t} + \boldsymbol{\nabla} \cdot (\bar{\boldsymbol{U}} \bar{\Sigma}') = \boldsymbol{\nabla} \cdot [\bar{\Sigma}' (\bar{\boldsymbol{U}} - \bar{\boldsymbol{U}}_{\Sigma'})] + \dot{\Sigma}'_{int} \tag{20}$$

Consequently, Σ' is solved using Equation 20, while Σ is calculated using Equation 19 and 14. The equation for the surface density is a postulated equation. Several source terms have been proposed in the literature but due to the lack of experimental data, theirs validities have still to be established. The present approach has been to use only the minimum source terms to be able to reproduce available data [4, 48] to keep a form of the equation as comprehensible as possible. Once the spray is dispersed the situation is different because there exist established models that can be rewrite in term of source terms for this surface density equation. Our proposal is to activate the dispersed source term once the dispersion is achieved [4] or to switch to a Lagrange formalism that is commonly used for dispersed spray and for which appropriate model are available. In this work, the dispersed part of the model is not activated because the focus is on the dense zone of the spray:

$$\dot{\Sigma}'_{int} = C_\Sigma \frac{\Sigma}{\tau_\Sigma} \left(1 - \frac{\Sigma}{\Sigma^*} \right) \quad , \tag{21}$$

which is based on an equilibrium value of surface density, Σ^* that should be reached within a characteristic time scale, τ_Σ. C_Σ is a constant that is set equal to 0.4. C_Σ is a model constant and its value might effect the prediction of Σ. In the initial works (for example [4, 1]) C_Σ was set to 1 because of lack of relevant information. Later, Duret et al. [48] performed DNS with various configurations of liquid volume fractions and surface tension values to quantify this parameter. Following his work, a value of $C_\Sigma = 0.4$ was found to provide the best match between DNS and the modeled surface density Σ. Σ^* is given by the Weber number at equilibrium that can be obtained from the work of Duret et al. [48]. Finally the modeled equation for Σ' becomes:

$$\frac{\partial \bar{\Sigma}'}{\partial t} + \boldsymbol{\nabla} \cdot (\bar{\boldsymbol{U}} \bar{\Sigma}') = \boldsymbol{\nabla} \cdot \left[\frac{\nu_t}{Sc_t} \boldsymbol{\nabla} \bar{\Sigma}' \right] + C_\Sigma \frac{\Sigma}{\tau_\Sigma} \left(1 - \frac{\Sigma}{\Sigma^*} \right) \tag{22}$$

Further discussions of these terms are available in works of Vallet et al [2] and Lebas et. al [4], that proposes various forms of modeling terms. Here the purpose is to use first the simplest formulation and introduce complex models only when necessary. A length scale can be defined from Σ and α: $\frac{\alpha}{\Sigma}$, which is related to SMD. On the one hand, for mono-dispersed spray of spherical droplets, the SMD will have the following form: $\frac{6\alpha_l}{\Sigma}$. On the other hand, for very small volume fraction leading to bubbly flow: $SMD = \frac{6(1-\alpha_l)}{\Sigma}$. Finally, to account for all structures, a length scale l_{32} is derived, as $l_{32} = \frac{6\alpha(1-\alpha)}{\Sigma}$.

3. Numerical Test Case

The previous sections have described different available approaches to address the liquid-gas turbulent flow within dense zones (i.e., non-dispersed or primary atomization). One aim of these approaches is to conduct simulation of fuel injection for which a comprehensive data base has been set up by the ECN group of research[49]. To simulate numerically these fuel injection system, a full ICM-DNS approach should give the best comparison with experimental data but it is not affordable for the time being, therefore models are mandatory. A numerical representation based on full ICM-DNS for the initial destabilization of the complex turbulent liquid jet going up to the spray formation for which well established numerical model can be used is appealing but has not yet been applied. Indeed such an approach requires the ICM-DNS to be applied up to the formation of each individual droplet that would require too much CPU resources. Hence, in many situation models have to be applied for the dense turbulent liquid-gas flow, among them the *ELSA* approach has been successfully applied using the Favre formulation on an ECN database [49] by several teams [50, 51, 37] mainly in the RANS context leading to CPU cost compatible with industrial application. The purpose of the following test cases is to extend the analysis considering complementary approaches based on Reynolds averaging. In addition, comparisons between RANS and LES for the dynamics of the flow

are conducted together with an analysis of the numerical model used to represent the interface, in particular for the LES approach. For this latest aspect, the interface can be considered to be captured at the mesh resolution (ICM approach) or the interface can be considered at subgrid level (diffuse interface approach) for which a turbulent subgrid liquid flux driven mainly by liquid dispersion has to be considered. The diffuse interface approach combined with the dispersion model has already been successfully tested by Chesnel et al [17] in another framework by comparison with DNS results. On the opposite view, a full ICM-DNS can be used assuming no liquid dispersion at the subgrid level. Finally, a coupled approach is also tested base on IRQ's sensors to determine locally and dynamically whether or not the interface is well captured.

Regarding the geometry, several options may be considered, from simple 2D axisymmetric configurations [50] up to full 3D simulations with injector flow and needle movement [37]. In both cases it has been possible to show that even with the less resolved modeling (RANS), the essential features of the injection can be captured with *ELSA* approach. An advantage of these ECN test cases is the possibility to simulate also the flow inside the injector. An axisymmetric test case was studied in a previous work [52]. Here, only 3D domains are considered, thus better representing three dimensional nature of turbulent eddies in particular for LES formulation. For 3D simulations a simplified geometry is considered. The 1D axial profile of the injector (210675) is taken from ECN website (red line on the Figure 1). The geometry was extended to include the injector sac and needle. The profile is then rotated to create a 3D mesh. A measured 3D geometry is also available from ECN database which has been obtained using high resolution x-ray tomography [53]. Results obtained using such a geometry are also reported at the end of section 4.

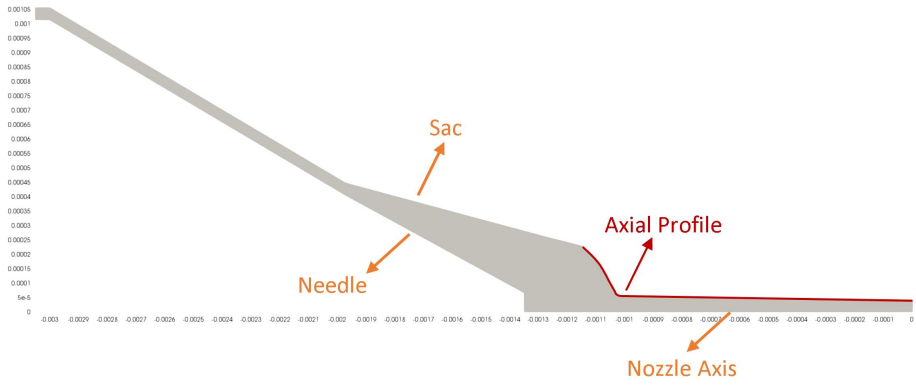

Figure 1: Injector profile used to make a simpled 3D geometry

For the Simplified Geometry two meshes has been studied. One *coarse* mesh to get quicker results and another *fine* mesh to see the fluctuating interactions with the interface. For the latter case, and with initial estimates of velocity profiles from ECN experimental results, the Taylor length scale [54] was used, which can be calculated following the equation below:

$$\lambda_g = D_{inj}\sqrt{10}Re_{D_{inj}}^{-\frac{1}{2}} \quad , \tag{23}$$

which gives $\lambda_g \approx 1.26 \times 10^{-6} m$. The *fine* mesh has cell size of about $1\mu m$ at the exit of the injector. The mesh size was increased gradually to about 12 μm at the end of the chamber. The total length of the domain after the injector exit is 10 mm. The details of mesh parameters are shown in Table 1.

Table 1: 3D Meshes

	Cells at the Nozzle Exit	Total Number of Cells (M)
Simplified Geometry (Coarse)	56	4.85
Simplified Geometry (Fine)	98	32

The cross-section of meshes for the simplified geometry is shown in the Figures 2 & 3.

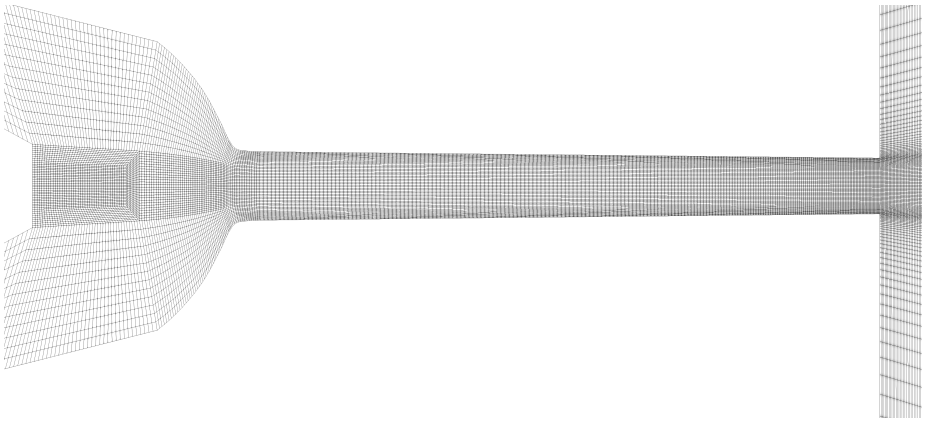

Figure 2: A transverse section of the Mesh. Shown here is coarse (56 cells at the nozzle exit, Total 4.85 M cells). Fine mesh (not shown here) has 98 cells at the nozzle exit with a total of 32.28 M cells

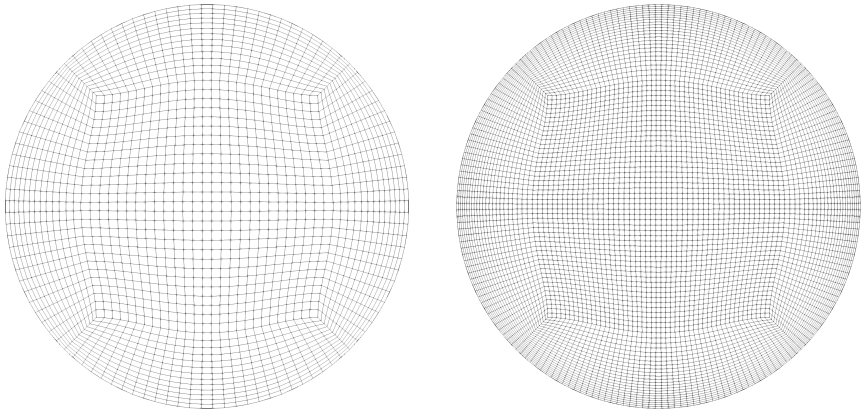

Figure 3: Mesh at nozzle exit. Left: Coarse mesh, Right: Fine mesh

In reality, the injector also includes an axial displacement of the needle [37]. Nevertheless, transient mass flow rate inlet boundary condition allows to reproduce partly the effects of the needle motion [50, 51, 55]. In compressible formulation one can also use time varying total pressure inlet boundary condition to mimic the actual flow development [56]. Nonetheless, the established

jet, which is the main subject of this study, can be obtained directly with a constant mass flow rate inlet [57]. The first comparison will be based on this simplified test case. Accordingly, operating conditions for typical ECN Spray A are reported in Table 2.

Table 2: Conditions for non-evaporating ECN Spray A [49]

Fuel	n-Dodecane
Ambient composition	100% N2
Injection pressure [MPa]	150
Ambient pressure [MPa]	2
Ambient temperature [K]	303
Ambient density [kg/m^3]	22.8
Fuel injection temperature [K]	343

From the previously described models and depending on the equations solved, there are several possibilities: Initially, RANS and ELSA (diffused interface) model using RANS were tested, namely `ELSAFoam` solver. Likewise, LES and ELSA using different turbulence models, such as WALE and Smagorinsky. The effect of mesh resolution and type of LES model is also important, thus we have simulated two meshes and two different LES models. Results based on Favre averaging have already been reported previously [50, 51, 37]. Additionally, LES with ICM analysis using WALE turbulence model, namely `interFOAM` solver was also examined. In the end, LES coupled with dynamic switching between ICM and ELSA based on IRQ's, namely `icmELSAFoam` solver was verified. Summary of all the configurations studied are shown in Table 3.

Results reported here focus on the established flows, thus simulations were performed with constant mass flow rate inlet boundary condition that have been conducted until a statistically steady-state is obtained. For the chamber, outflow boundary condition is used. While for the chamber tip, i.e. the surface adjacent to the injector exit, is treated as wall. A total pressure boundary condition is imposed on the outlet and chamber patches. Σ' is modeled with zero gradient

Table 3: Different cases set-up.

Solver	Equations solved	Coarse Mesh	Fine Mesh
		RANS ($k-\varepsilon$)	RANS ($k-\varepsilon$)
`ELSAFoam`	Eqns. 8 and 4	LES (Smag.)	LES (Smag.)
		LES (WALE)	LES (WALE)
`interFoam`	Eqn. 12, C_α = *1*	LES (WALE)	LES (WALE)
`icmELSAFoam`	Eqn. 12, C_α *adaptive 0 or 1*		LES (WALE)

type boundary condition for all boundaries (outlets), except at the inlet where its value is set equal to zero. Second order backward time scheme is used for all quantities except for α, for which a special procedure called MULES is used to preserve boundedness of this quantity. This special treatment is applied for the liquid volume fraction in order to keep it bounded [24], besides, local sub-cycling of phase fraction equation is possible and in this work three local sub-cycles are used. The time-step is limited by Courant number Co and Interface Courant number $Co_{interface}$, which is defined on near interface regions as:

$$Co_{interface} = pos(\alpha_l - 0.01)pos(0.99 - \alpha_l)\max\left(\frac{|\boldsymbol{U}|}{\Delta x}\right)\Delta t \tag{24}$$

where $pos(x)$ is a mathematical function which returns 1, if x is greater than 0 and 0 otherwise. The maximum Co and $Co_{interface}$ is set to 0.25. The time-step is adjusted automatically to limit the Courant number below the imposed constraint, which resulted in a time-step between 2×10^{-10} s to 3×10^{-10} s on the fine mesh.

4. Results and discussion

The data available from ECN website in the form of Liquid Volume Fraction (LVF), Projected Mass Density (PMD) and Transverse Integrated Mass (TIM) is used for validation purpose and to compare the impacts of different modeling approaches. Note that LVF data are obtained from PMD measurement with a mathematical transformation [58] that assumed axisymmetrical flow in average.

4.1. Validation

A comparison process has been made against experimental and numerical data available from the Engine Combustion Network (ECN) in order to validate the proposed ELSA model. The Spray-A non evaporating configuration has been selected, with exact aforementioned fluid properties. The experimental data used for validation include the PMD of the fuel, which was obtained by a line-of-sight integration along the x-ray radiography measurement [59, 60], and the TIM, which was acquired from the integral of the projected density across a transverse position at a particular axial location [61].

In order to characterize the bulk flow inside the injector, nozzle coefficients are used and are often quoted by the manufacturers. These include discharge coefficient, C_d, velocity coefficient, C_v, and area coefficient, C_a. See equation (25) and reference [62] for more details in their implementation. The idea is based on measuring average quantities, like mass flow rate and momentum flux and use them to compare with theoretical formulations without considering any pressure losses. The discharge, velocity, and area coefficient are computed respectively as:

$$\begin{cases} C_d = & \frac{\dot{m}}{\dot{m}_{th}} \quad , \\ C_v = & \frac{u_{eff}}{u_{th}} \quad , \\ C_a = & \frac{A_{eff}}{A_o} \quad . \end{cases} \tag{25}$$

Finally, one can derive that

$$C_d = C_v C_a \quad . \tag{26}$$

In the Table 4, results for several simulated cases are shown. Since there is no interface inside the injector (i.e. single phase flow) the corresponding interface models are not repeated here, hence only results obtained with `ELSAFoam` are reported. It can be seen that the results of C_d and C_a are within the measurement uncertainty of experimental data even on coarse mesh. Thus, increasing the mesh size does not produce any significant change on these values. LES

WALE model on fine mesh, however, predicts the nominal value with much more confidence as far as experimental data are concerned.

Table 4: Nozzle discharge and area coefficients for different cases

	C_d	C_a
ECN Exp.	0.90±0.01	0.98±0.02
RANS ($k-\varepsilon$) Coarse	0.888	0.983
RANS ($k-\varepsilon$) Fine	0.887	0.972
LES (Smagorinsky) Coarse	0.8875	0.966
LES (Smagorinsky) Fine	0.887	0.952
LES (WALE) Coarse	0.888	0.984
LES (WALE) Fine	0.896	0.981

In order to better visualize the impact of different models, Figure 4 shows velocity magnitude scaled to an equal value for all the simulations. RANS has already reached convergence with the coarse mesh. Consequently, further increasing the mesh size does not produce any new information. Smagorinsky model is not able to capture any turbulence at the exit of the injector, even after the first twenty diameters of injector (at 2 [mm]). Because of very high Re number ($\approx 5.7 \times 10^4$) it is expected to have a turbulent flow at nozzle exit (right edge of figure 1) as also reported in [63]. To have a clear difference of LES model, visualization of flow field at nozzle exit using fine mesh is shown in Figure 5. The top half shows the slice of velocity field at nozzle center plane obtained using Smagorinsky model, while the bottom half shows the one obtained using WALE. In-nozzle turbulent flow field fluctuations are predicted by WALE model as expected in contrast to Smagorinsky model where no such fluctuations are captured. By using an even finer mesh with Smagorinsky model tending to a DNS approach, results may be comparable, however such a study is outside the scope of this work. Turbulence captured by WALE model also have pronounced effect on surface perturbations at the exit of the injector, as shown by the velocity field within first few diameters downstream injector. Thus, in the later

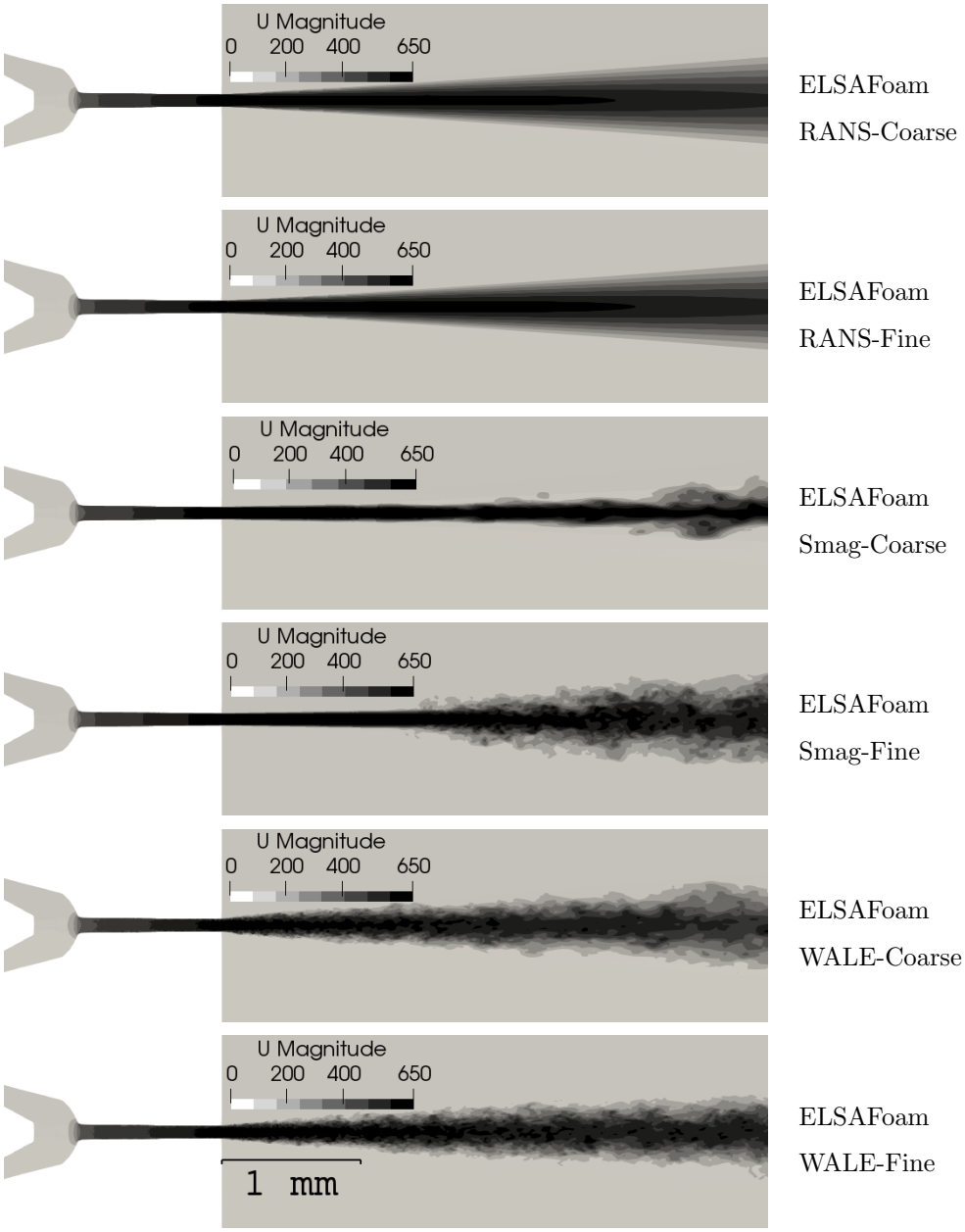

Figure 4: Instantaneous velocity magnitude for different cases

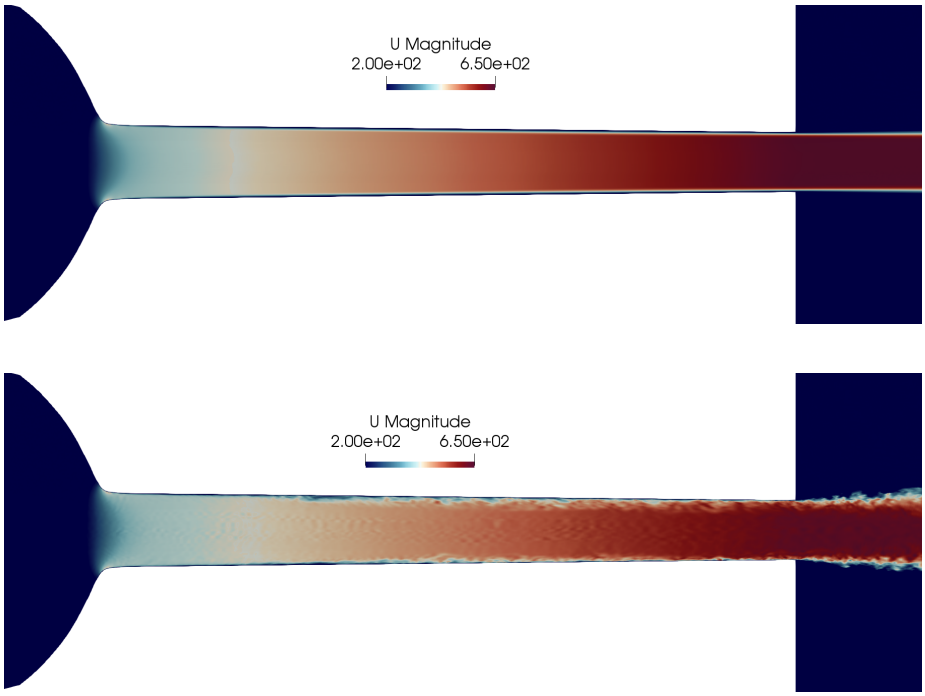

Figure 5: Effect of LES model on velocity. Velocity at nozzle center plane. Range is limited to enhance visualization. Top: Smagorinsky, bottom: WALE model with the identical fine mesh. On the right edge of figure, the blue region indicates the start of ambient atmosphere, where nitrogen is initially assumed at rest.

part of this paper no results for Smagorinsky model are further discussed. On the other hand, WALE model is able to capture the internal nozzle flow velocity fluctuations even with *coarse* mesh, thus giving the opportunity for turbulence inside the jet to be developed. The effect of refining the mesh is not very pronounced here, however, decreasing the mesh size helps in resolving small-scale vortex structures as shown in Figure 6. At the beginning of the nozzle there are no significant differences between the meshes, however, at the exit, an increased vortex structures appear near the wall, which means an enhanced (better resolved) turbulent kinetic energy gradient is being obtained.

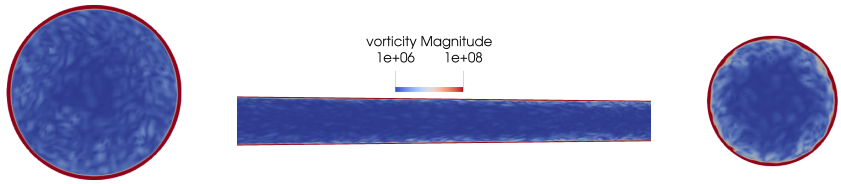

(a) Inlet x-section (b) Nozzle center plane (Coarse mesh) (c) Exit x-section

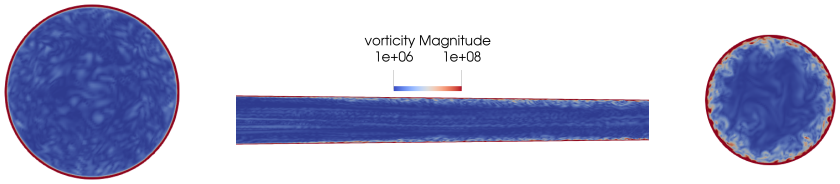

(d) Inlet x-section (e) Nozzle center plane (Fine mesh) (f) Exit x-section

Figure 6: Vorticity at nozzle transverse plane (center) and cross-section at the inlet (left) and exit (right) of nozzle using LES-WALE on coarse (Top) and fine mesh (Bottom). Nozzle dimensions are zoomed in.

The instantaneous LVF of established jet is shown in Figure 7. In RANS, increasing the mesh size does not bring any new information. The results of LVF obtained with coarse and fine mesh indicates the basic shortcoming of RANS in multiphase flows. One cannot expect to obtain any further information just by increasing the mesh size. LES on the other hand, tends to DNS as we keep on refining the mesh by decreasing the dependency on modeling terms. With LES and WALE model, ELSA relies on subgrid modeling, thus decreasing mesh size decreases the dependency on subgrid modeling.

In-contrast, `interFoam` is developed on the ideology of capturing the interface and keeping it sharp, which is a physically correct approach, but is limited to mesh resolution. If the mesh is not fine enough, the model produces diffused interface which is basically a numerical diffusion. This is clearly visible in Figure 7 on fourth and fifth row, we can see the effect of refining mesh changes the volume fraction field significantly. Liquid core appears to be attached for longer

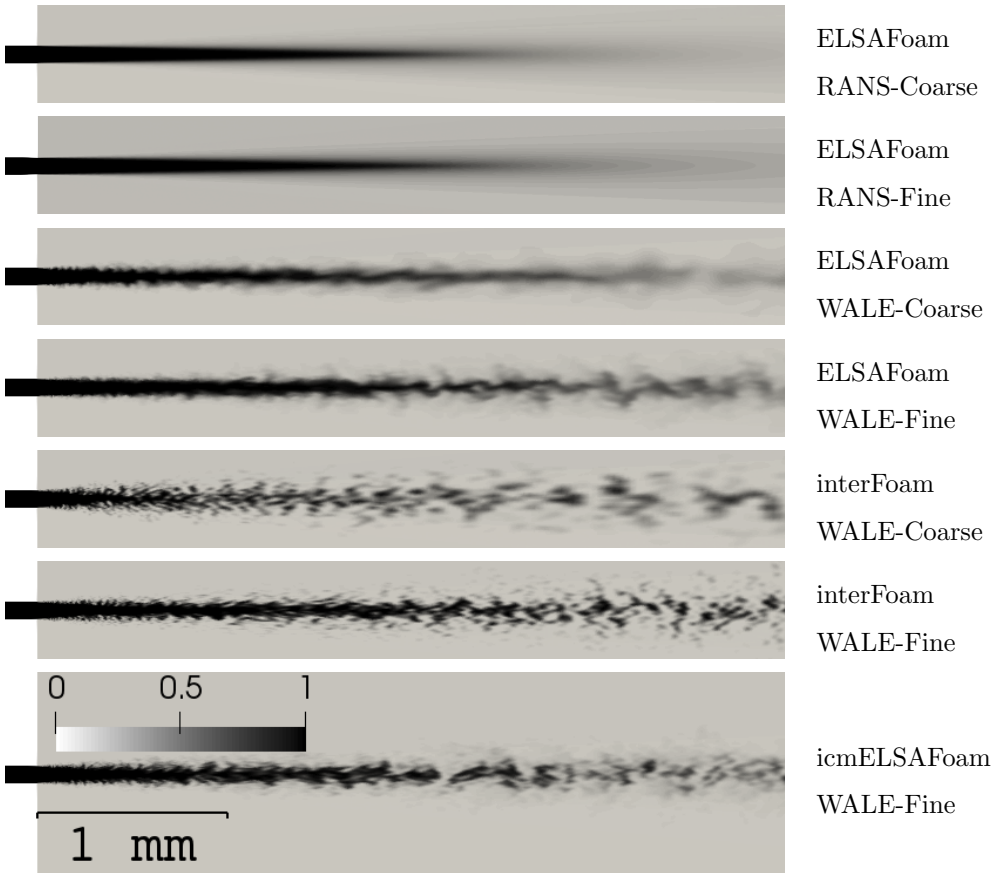

Figure 7: Instantaneous liquid volume fraction for different cases

length and individual small packets of fluid are captured as well. However, there is no certain way to tell when the numerical diffusion is more dominant, especially towards the end of domain where the mesh size is increased gradually. We have thus proposed a methodology to identify this by using IRQ criteria introduced previously. Consequently, `icmELSAFoam` gives an intermediate result between `interFoam` within the first millimeter and `ELSAFoam` result in the last part, which is in fact, the expected behavior of the model.

A quantitative analysis for mean LVF is shown in Figure 8. The top row in Figure 8 shows results obtained using coarse mesh, and those with fine mesh are

shown in the bottom row. At 0.1 mm from the exit of injector, all the models predict almost same results, as the mesh is relatively fine at this location. LES however, shows some spreading of the jet at the periphery, indicated by curved tails at the ends. At 2 mm with the coarse mesh, Figure 8(a), `interFoam` fails to predict the experimental mean LVF profile, indicating that a finer mesh is required. This is indeed verified in Figure 8(b) where a refined mesh produces expected results. The sub-grid modeling of `ELSAFoam` helps to achieve reasonable results even on a coarse mesh. Refining the mesh further produces a better experimental match. At 6 mm on coarse mesh it seems the numerical diffusion produced by `interFoam` gives the same results as predicted by subgrid modeling, `ELSAFoam`. This is however, a mere coincidence, since even with fine mesh `interFoam` cannot capture all the flow physics as verified by the unphysical high value peak of LVF, Figure 8(b). From this discussion, it is emphasized on the point that, interface capturing methods (`interFoam` and others such as level set [5], ghost-fluid [28], level set coupled with VOF method [64]) are very good as far as the mesh requirements are met. Once the mesh is not refine at satisfactory level, the results obtained are not very reliable because there are linked to uncontrolled numerical errors. In the case of `interFoam` this error appears like a a numerical diffusion that is confusing because it may represent well in some case the subgrid dispersion. However, this numerical error lead to result that are dependent of the mesh resolution. Other ICM approaches, that always preserve a sharp interface such as based on Level Set Method limit spray dispersion at the grid resolution and then neglected the subgrid liquid dispersion [17] bringing an other kind of numerical error also leading to mesh resolution dependency. To address subgrid liquid dispersion it is better to rely on physically based subgrid modeling and to take advantage of ICM where the mesh resolution is high enough.

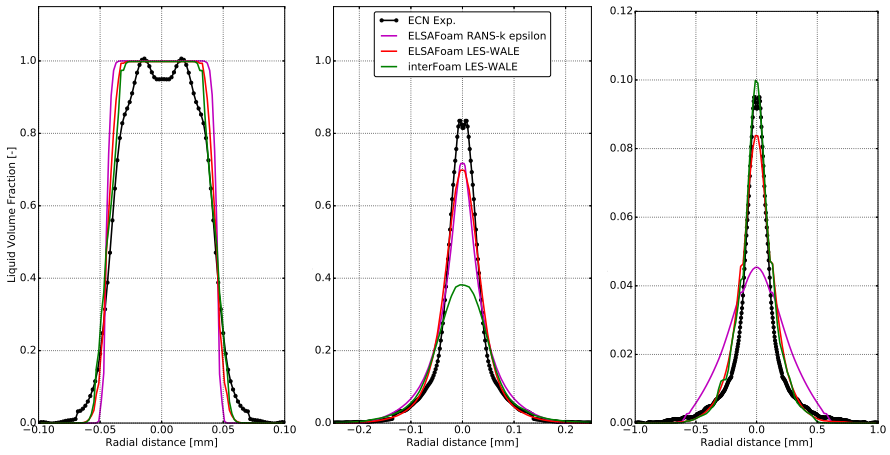

(a) Coarse mesh

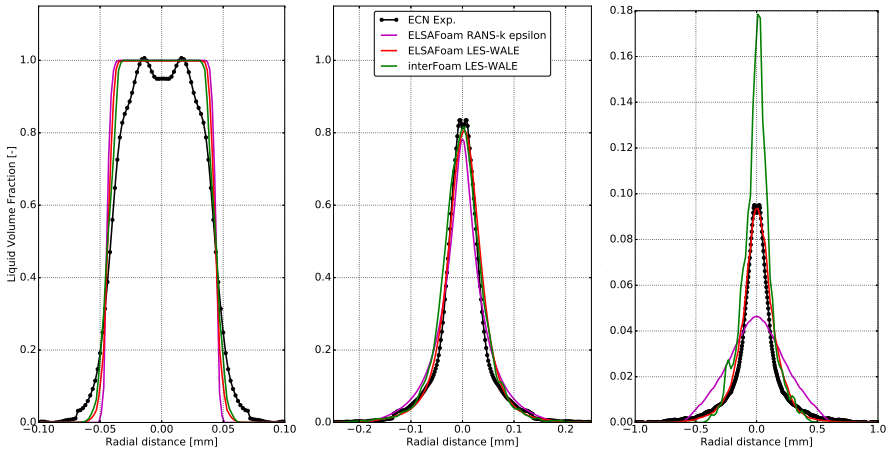

(b) Fine mesh

Figure 8: Mean LVF radial profiles at 0.1 mm (left), 2 mm (center) and 6 mm (right)

This particular feature is highlighted in figure 9, which shows the contour of LVF for diffused interface and interface capturing techniques. The diffused interface approach dumps the fluctuation in the LVF field, hence surface tension dominated effects might not be captured, and force the field of the liquid core to remain attached or in other words, diffused. On the other hand, some ligaments and pockets of liquid get detached from the liquid core using ICM. The breakup

process at this scale is handled well by interface capturing methods if the mesh resolution is fine enough.

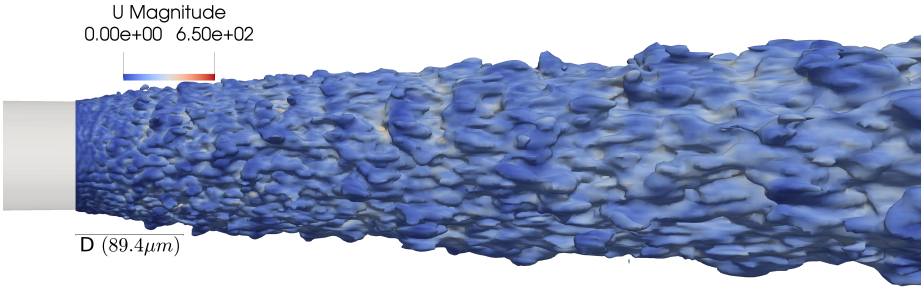

(a) Diffused interface (`ELSAFoam`)

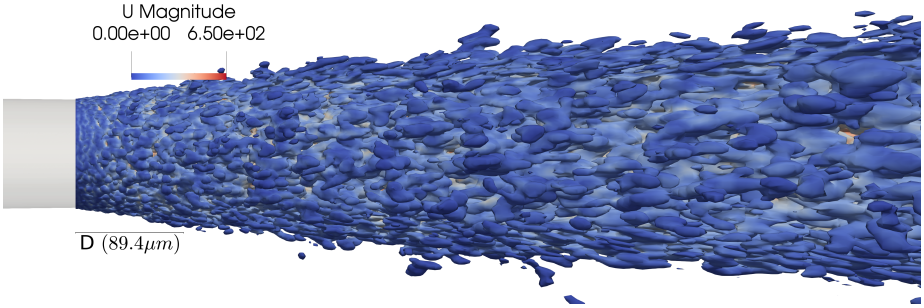

(b) Interface capturing method (`interFoam`)

Figure 9: Contour of $\alpha_l = 0.01$ with diffused interface and interface capturing method.

Along the same line of thought, `icmELSAFoam` (see equation 12) is introduced to switch off the ICM when sub-grid fluctuations become important and use the ICM when mesh density supports such implementation. The PMD (from which the LVF has been extracted) is now directly used to compare the numerical results with the experimental ones from ECN data base.

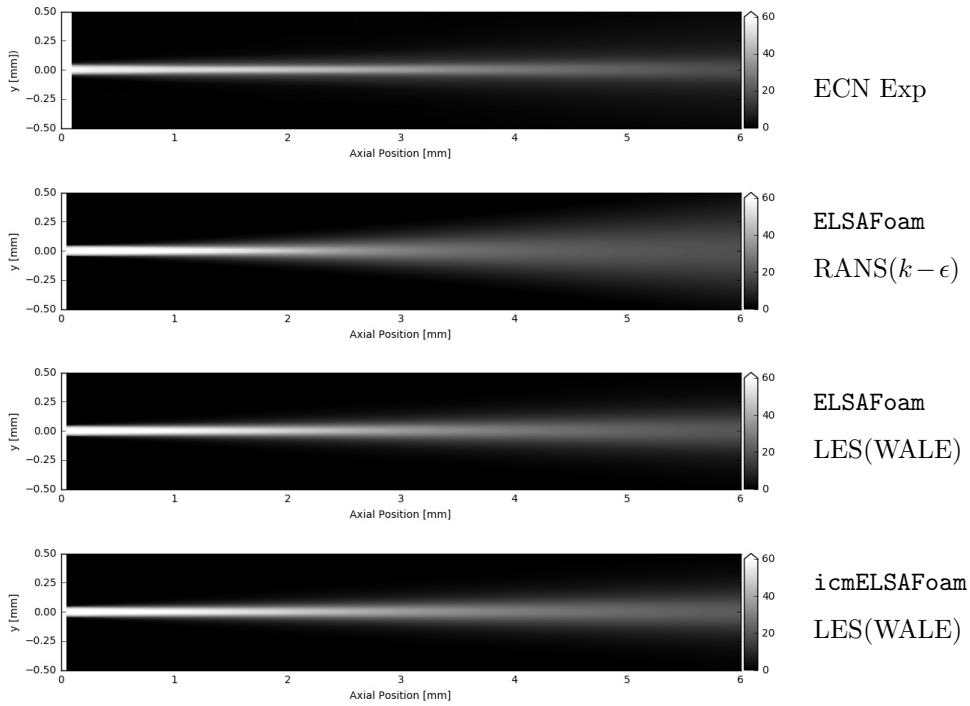

Figure 10: PMD results (in $\mu g/mm^2$) for different cases with fine mesh

Figure 10 clearly shows RANS's result being the most diffusive, thus underpredicting the liquid penetration. On the other hand, much better and comparable results are obtained with both `ELSAFoam` and `icmELSAFoam`, for the liquid penetration and dispersion. Additionally, there are not observed appreciable differences between both solvers. Hence, a better way to visualize PMD, is a qualitative radial profile at various axial distance from the exit of the injector. The results for *fine* mesh for such computations are shown in Figure 11.

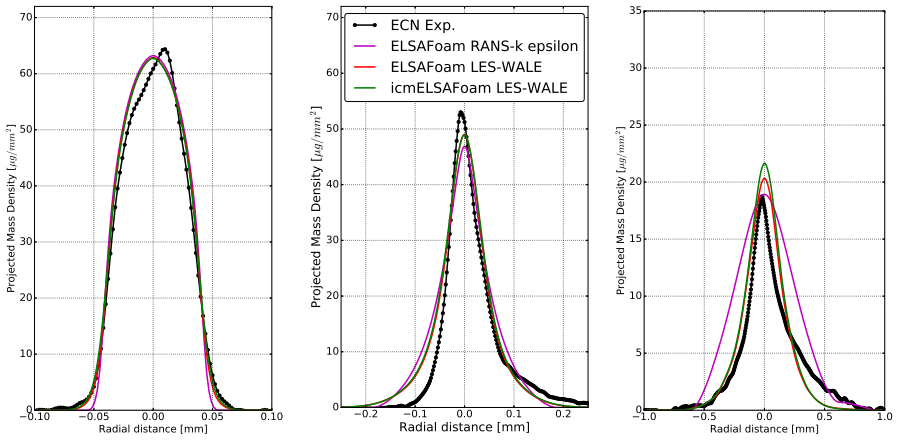

Figure 11: PMD radial profiles at 0.1 mm (left), 2 mm (center) and 6 mm (right) for fine mesh

Firstly, at 0.1 mm all models present the same profiles. Again LES is able to capture the details of flow stretching at the periphery of jet due to a better description of the turbulent flow field. Thus instead of a straight line profile at the two tails of the PMD curve, a curved profile is predicted as indicated by experiments as well. Secondly, at 2 mm (nearly 20 times the injector diameter) there are no considerable differences between `ELSAFoam` and `icmELSAFoam` which indicate the presence of large fluctuations in the near-field spray. This is mainly due to the high turbulence coming from the inlet conditions and also from the shear stress with the surrounding gas which is highest at the vicinity of the injector exit. Thirdly, at 6 mm (60 diameters from the exit), even if differences are small, `ELSAFoam` is the one that matches the best compared with experiments with a little more over-penetration to `icmELSAFoam`. Apparently, the fluctuations decrease within the dilute/dispersed zone more than it should.

A useful parameter might help to perceive the sub-grid dominance within this zone: C_α, defined in equation 12, equals one (1) when the interface is resolved and equals zero (0) otherwise. Figure 12 partially confirms that, just after a few millimeters after injector exit, the sub-grid scales become of paramount importance and the interface is diffused rapidly, mainly due to the high shear

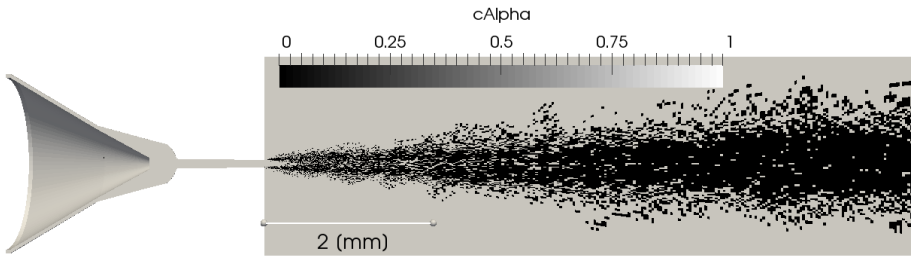

Figure 12: C_α colored map.

stress and turbulence at the interface liquid-gas that creates small wrinkling on the surface not captured by the actual *fine* mesh. To go further a better mesh resolution is necessary to keep track of the actual interface position further downstream of the liquid jet. For the present work, the area for which the interface is considered well captured by `icmELSAFoam` cover a very small range of the atomization process, just at the vicinity of the injector nozzle. Nonetheless this zone may be important to relate the in-injector flow characteristic to the initial destabilization of the liquid jet interface.

Transverse Integrated Mass (TIM), is another experimental quantity which represents the dispersion of the atomized liquid axially. A higher value indicates that at an axial position the amount of liquid all along the radial position is higher. This may be due to a high rate of liquid dispersion that spread away from the axis the liquid or due to a higher liquid penetration that keeps an important liquid amount on the axis. The results for TIM are shown in figure 13. As verified previously, RANS model exhibits the highest dispersion. `ELSAFoam`, `icmELSAFoam` produce comparable results and a noticeable improvement with respect to RANS approaches. Nonetheless, `icmELSAFoam` displays slightly higher value of TIM than `ELSAFoam`, which does not necessarily mean `icmELSAFoam` is more diffusive than `ELSAFoam`, but the integral of projected mass density (PMD), across the transverse axis at particular positions is higher, which is in agreement with figure 11, owing to greater liquid penetration at 6 [mm] for instance.

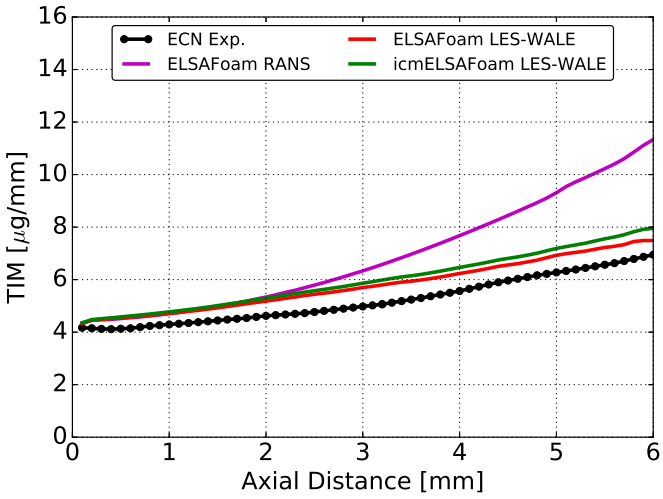

Figure 13: TIM for different cases with fine mesh

The improvement obtain by using LES with respect to RANS simulation are in line with results presented by Desantes at al. [36]. As for RANS they have used a mass weighted formulation for LES but the results are comparable to those presented in this work. Interestingly, they have used a synthetic turbulent inlet condition starting computation from the injector nozzle exit plane. One of these inlet model parameters is the turbulent intensity that they varied from 3% to 5%. This small change produced differences in terms of PMD or TIM that are of the same order of magnitude to those obtain in this work between `ELSAFoam` and `icmELSAFoam`. Since the main difference between these two approaches to the current test case is due to the liaison with the internal flow, it may be concluded that the model developed are sensible enough to capture the differences in nozzle flow conditions. Accordingly, the internal flow field description becomes a very important feature of the whole simulation.

To try to determine the internal flow field as best as possible the starting point is to get the actual geometry of the injector. An attempt was made to use the measured geometry (available from ECN database) of the injector, which has been obtained using high resolution x-ray tomography. The corresponding

mesh obtained using such a file is shown in Figure 14. The non circular nozzle exit as well as abrupt changes in nozzle cross-section are readily visible in Figure 14. Nevertheless, owning to the measurement uncertainty of the experimental apparatus combined with the variation in the nozzle diameter/sections of the order of a fraction of microns, a represented average profile cannot be obtained by one such measurement. Instead, a smoothing process is required based on detailed measurements of the nozzle exit diameter and specific sections to improve the geometry [53, 65]. In this case, only slight noise suppression was used to smooth the geometry.

It is to be noted that preprocessing of files obtained from tomography takes considerable time. Hence the decision to spend time on this aspect should depend on the expected quality of results and measurement uncertainty of experimental reconstruction algorithms. The most important fact regarding our experience to design such a mesh is the necessity to choose in between arbitrary parameters during the mesh construction and smoothing process. Consequently, the proposed mesh is only one possible representation of the geometry. Other choices during the mesh building process would have led to another approximation of the geometry. Available data despite the great effort performed by ECN network on this topic would not permit to discriminate the best solution to this problem. Authors of this work believe that this is one of the current limitation to go further on detailed simulations of such atomization process. It is also necessary to mention that the moving needle motion is not considered in this work which is, of course, also an important limitation regarding the internal flow even if results reported here concern the established flow.

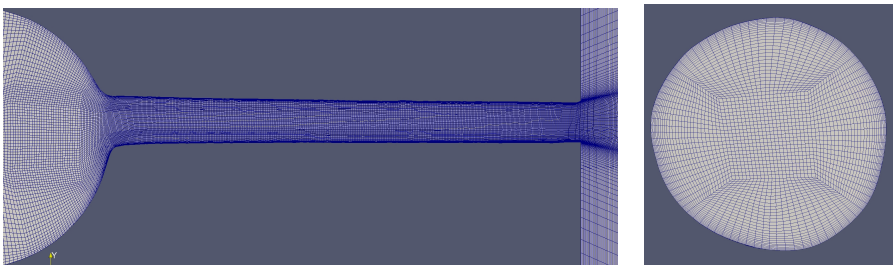

(a) Mesh Nozzle (b) Nozzle exit plane

Figure 14: Mesh from Stl file. Mesh with 82 cells at nozzle exit. Total number of cells: 5.35 M

The PMD profile obtained with this new internal geometry are reported on Figure 15. Due to the measured geometry that included very small features, the corresponding mesh includes small mesh cells that constrain the time step for numerical stability of the simulation. Consequently the total time of the simulation is increased and only the `ELSAFoam` approach has been used. The trend of shifted PMD with respect to center was captured to some extent but not completely. For the time being it is difficult to conclude which part of the model should be improved: geometry, mesh or physical modeling. Nonetheless, the simulation is slightly more accurate with the measured geometry instead of using the simplified asymmetric one.

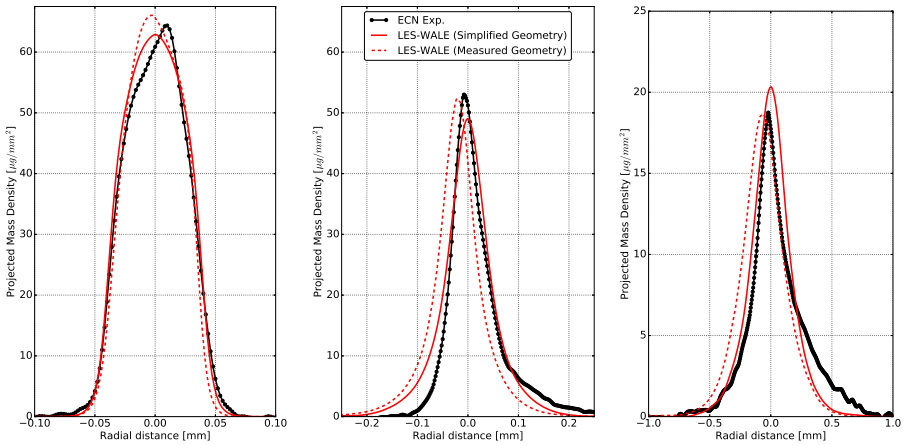

Figure 15: PMD at 0.1 mm (left), 2 mm (center) and 6 mm (right).

5. Conclusions

The present work concerns two approaches available to simulate liquid injection system in flow regimes characterized by high Reynolds and Weber numbers. The focus is on the description of the dense liquid-gas flows, where the spray is not yet formed. Though the area covered by this kind of turbulent liquid-gas flow is often small (less than a few diameters away from injector nozzle), it is mandatory to address it to link the inside injector flow to the final spray. It is recognized that DNS coupled with accurate ICM approaches are very valuable and accurate tools to describe this flow as soon as the mesh resolution is sufficient. This requires that the subgrid turbulent liquid flux can be neglected. It is also important to recognize that in many practical applications such level of mesh refinement is not affordable. Consequently, physical models able to represent the subgrid liquid dispersion are expected. Since the work of Vallet and Borghi [1], the main lines of the so-called ELSA model have been designed for this purpose. The turbulent liquid-gas flow is the place of strong density variation. Following the original formulation of Vallet and Borghi, many works have been conducted using Favre mass weighted averaging and filtering. The present work completes these frameworks by considering Reynolds volume averaging

and filtering approach. This work has shown that the volume formulation can be used and give comparatively as accurate results as the previous mass formulations with respect to available experimental data despite approximation done in both formulations. A benefit of the volume formulation is to keep the liquid volume fraction as a primary variable transported by the model like in many Interface Capturing Methods (ICM) belonging to the VOF family. Accordingly, a set of models is designed based on ELSA framework for different levels of refinement. A volume-based formulation, namely ELSA approach, has been implemented using the OpenFOAM® library, leading to the solver `ELSAFoam`, that can be applied using both RANS and LES model for turbulence modeling. This model considers a possible subgrid turbulent liquid flux that depends on the local flow condition. The important point is the incompatibility with ICM numerical method that preserved a sharp interface representation. Thus, even when the interface is well resolved the turbulent liquid flux vanishes but the numerical method, not designed to capture the interface, prevent to recover the accuracy of ICM approaches. To solve this problem two criteria for interface resolution quality (IRQ) have been proposed to determine dynamically if the subgrid turbulent liquid flux has to be considered coupled with a standard numerical method or if the resolution of the interface is good enough to neglect interface subgrid effect and thus to apply ICM. The corresponding solver based on the OpenFOAM® library has been called `icmELSAFoam`. The original surface density equation [1] has been extended for all developed formulations.

The second part of the paper is devoted to the analysis of the proposed approach with respect to the experimental data based developed by the ECN [49] research initiative. In particular experimental data from x-ray radiography measurements of non-evaporating Spray A condition have been used. Like previous work based on mass formulation a global agreement has been obtained with respect to the available data, namely: liquid volume fraction, projected mass density and transverse integrated mass. In particular, even RANS formulation that can be very cheap in term on CPU consumption when using axisymmetric mesh, is able to reproduce the global behavior of the injection. Nevertheless, to recover

the actual dispersion of the liquid a real improvement can be obtained using LES formulation with both solvers `ELSAFoam` and `icmELSAFoam`. Accordingly, a 3D mesh with a high resolution in the injector nozzle is required. In particular, the turbulence inside the nozzle is mainly controlled by the development of a turbulent boundary layer starting from the internal nozzle cavity that develops until the end of the injector pipe. To capture this phenomenon, mesh refinement along the injector nozzle wall combined with an appropriate LES-WALE model has been necessary. This turbulent boundary layer interacts directly with the liquid-gas interface at the exit of the injector to initiate the atomization process. This phenomenon is well captured only with ICM approaches, in particular with the `interFoam` solver. Nevertheless, further downstream as the atomization process continues, the length scale of interface wrinkling decreases continuously leading to a numerical error in ICM approaches. By changing mesh resolution, it has been shown that this numerical error is driving the liquid dispersion. This mesh dependency can be released by considering subgrid scale effect with both solvers `ELSAFoam` and `icmELSAFoam`. Thus, it is better to use a physically based model for subgrid turbulent liquid flux than to rely on numerical error of ICM (if unresolved) to recover a mesh-independent result. Finally, the detailed simulation is sensible enough to relate the liquid dispersion to the internal flow inside the injector. Accordingly, an attempt has been made to use the measured geometry provided by ECN database. This approach introduces new difficulties because of geometrical measurement uncertainties and because of the necessary choices that have to be made during the meshing process to preserve or to smooth any details of the measured geometry. These bias, due to geometry uncertainties, meshing choices and model approximations, leads to noticeable modification of the liquid distribution that makes errors of few percents with respect to measured data. For the time being it is not easy to conclude which of these bias are the most important, but the positive conclusion is that the present models are sensible enough to detect these small changes. Main prospects of this work are twofold: firstly to test `icmELSAFoam` solver on injection with lower Reynolds and Weber number to recover a bigger area where the interface is well captured;

secondly, to test the behavior of the model with respect to the surface density prediction with respect to available data.

6. Acknowledgements

This work was partly supported by European Union's Horizon 2020 research and innovation program under the Marie Sklodowska-Curie grant agreement N^o 675676. This work was granted access to the HPC resources of IDRIS, TGCC and CINES under the allocation A0032B06153 made by GENCI (Grand Equipement National de Calcul Intensif).

7. References

[1] A. Vallet, R. Borghi, Modélisation eulerienne de l'atomisation d'un jet liquide, Comptes Rendus de l'Académie des Sciences-Series IIB-Mechanics-Physics-Astronomy 327 (10) (1999) 1015–1020.

[2] A. Vallet, A. Burluka, R. Borghi, Development of a eulerian model for the atomization of a liquid jet, Atomization and Sprays 11 (6) (2001) 619 – 642. doi:10.1615/AtomizSpr.v11.i6.20.

[3] H. G. Weller, G. Tabor, H. Jasak, C. Fureby, A tensorial approach to computational continuum mechanics using object-oriented techniques, Computers in physics 12 (6) (1998) 620–631.

[4] R. Lebas, T. Menard, P.-A. Beau, A. Berlemont, F.-X. Demoulin, Numerical simulation of primary break-up and atomization: Dns and modelling study, International Journal of Multiphase Flow 35 (3) (2009) 247–260.

[5] T. Menard, S. Tanguy, A. Berlemont, Coupling level set/vof/ghost fluid methods: Validation and application to 3d simulation of the primary break-up of a liquid jet, International Journal of Multiphase Flow 33 (5) (2007) 510 – 524.

[6] J. Shinjo, A. Umemura, Simulation of liquid jet primary breakup: Dynamics of ligament and droplet formation, International Journal of Multiphase Flow 36 (7) (2010) 513 – 532.

[7] J. Shinjo, A. Umemura, Surface instability and primary atomization characteristics of straight liquid jet sprays, International Journal of Multiphase Flow 37 (10) (2011) 1294 – 1304.

[8] F. A. Williams, Spray combustion and atomization, The Physics of Fluids 1 (6) (1958) 541–545.

[9] G. Bird, Molecular gas dynamics and the direct simulation of gas flows, Oxford University Press, 1994.

[10] F. Laurent, M. Massot, Multi-fluid modelling of laminar polydisperse spray flames: origin, assumptions and comparison of sectional and sampling methods, Combustion Theory and Modelling 5 (4) (2001) 537–572. arXiv:http://dx.doi.org/10.1088/1364-7830/5/4/303.

[11] F. Laurent, A. Sibra, F. Doisneau, Two-size moment eulerian multi-fluid model: a flexible and realizable high-fidelity description of polydisperse moderately dense evaporating sprays, Communications in Computational Physics 20 (4) (2016) 902–943.

[12] C. Yuan, F. Laurent, R. Fox, An extended quadrature method of moments for population balance equations, Journal of Aerosol Science 51 (2012) 1 – 23.

[13] D. A. Drew, S. L. Passman, Theory of multicomponent fluids, Vol. 135, Springer Science & Business Media, 2006.

[14] G. Blokkeel, B. Barbeau, R. Borghi, A 3d eulerian model to improve the primary breakup of atomizing jet, Tech. rep., SAE Technical Paper (2003).

[15] A. Andreini, C. Bianchini, S. Puggelli, F. Demoulin, Development of a turbulent liquid flux model for eulerian–eulerian multiphase flow simulations, International Journal of Multiphase Flow 81 (2016) 88–103.

[16] P.-A. Beau, M. Funk, R. Lebas, F.-X. Demoulin, Applying quasi-multiphase model to simulate atomization processes in diesel engines: Modeling of the slip velocity, Tech. rep., SAE Technical Paper (2005).

[17] J. Chesnel, J. Reveillon, T. Menard, F.-X. Demoulin, Large eddy simulation of liquid jet atomization, Atomization and Sprays 21 (9) (2011) 711–736.

[18] H. K. Versteeg, W. Malalasekera, An introduction to computational fluid dynamics: the finite volume method, Pearson Education, 2007.

[19] P. Sagaut, Large eddy simulation for incompressible flows: an introduction, Springer Science & Business Media, 2006.

[20] J. Smagorinsky, General circulation experiments with the primitive equations: I. the basic experiment, Monthly weather review 91 (3) (1963) 99–164.

[21] F. Nicoud, F. Ducros, Subgrid-scale stress modelling based on the square of the velocity gradient tensor, Flow, turbulence and Combustion 62 (3) (1999) 183–200.

[22] F. Ducros, F. Nicoud, T. Poinsot, Wall-adapting local eddy-viscosity models for simulations in complex geometries (1998).

[23] C. E. Brennen, Fundamentals of multiphase flow, Cambridge university press, 2005.

[24] H. G. Weller, A new approach to vof-based interface capturing methods for incompressible and compressible flow, OpenCFD Ltd., Report TR/HGW 4 (2008) 10.

[25] F. Raees, D. Van der Heul, C. Vuik, Evaluation of the interface-capturing algorithm of openfoam for the simulation of incompressible immiscible two-phase flow, Reports of the Department of Applied Mathematical Analysis 11 (7) (2011) 43.

[26] C. Hirt, B. Nichols, Volume of fluid (vof) method for the dynamics of free boundaries, Journal of computational physics 39 (1) (1981) 201–225.

[27] M. Sussman, P. Smereka, S. Osher, A level set approach for computing solutions to incompressible two-phase flow, Journal of Computational physics 114 (1) (1994) 146–159.

[28] R. P. Fedkiw, T. Aslam, B. Merriman, S. Osher, A non-oscillatory eulerian approach to interfaces in multimaterial flows (the ghost fluid method), Journal of computational physics 152 (2) (1999) 457–492.

[29] D. W. Lee, R. C. Spencer, Photomicrographic studies of fuel sprays (1934) 215–239.

[30] R. E. Phinney, The breakup of a turbulent liquid jet in a gaseous atmosphere, Journal of Fluid Mechanics 60 (04) (1973) 689–701.

[31] J. W. Hoyt, J. Taylor, Waves on water jets, Journal of Fluid Mechanics 83 (01) (1977) 119–127.

[32] D. Ervine, H. Falvey, Behaviour of turbulent water jets in the atmosphere and in plunge pools., Proceedings of the Institution of Civil engineers 83 (1) (1987) 295–314.

[33] G. Faeth, L.-P. Hsiang, P.-K. Wu, Structure and breakup properties of sprays, International Journal of Multiphase Flow 21 (1995) 99–127.

[34] F.-X. Demoulin, P.-A. Beau, G. Blokkeel, A. Mura, R. Borghi, A new model for turbulent flows with large density fluctuations: Application to liquid atomization, Atomization and Sprays 17 (4) (2007) 315–345.

[35] H. Jasak, Error analysis and estimation for the finite volume method with applications to fluid flows. (1996) 396.

[36] J. M. Desantes Fernández, J. M. García Oliver, J. Pastor, A. Pandal, B. Naud, K. Matusik, D. Duke, A. Kastengren, C. Powell, D. Schmidt,

Modelling and validation of near-field diesel spray cfd simulations based on the σ-y model, in: Ilass Europe. 28th european conference on Liquid Atomization and Spray Systems, Editorial Universitat Politècnica de València, 2017, pp. 98–105.

[37] Q. Xue, M. Battistoni, C. Powell, D. Longman, S. Quan, E. Pomraning, P. Senecal, D. Schmidt, S. Som, An eulerian cfd model and x-ray radiography for coupled nozzle flow and spray in internal combustion engines, International Journal of Multiphase Flow 70 (2015) 77–88.

[38] S. Pope, An explanation of the turbulent round-jet/plane-jet anomaly, AIAA journal 16 (3) (1978) 279–281.

[39] A. Pandal, R. Payri, J. García-Oliver, J. Pastor, Optimization of spray break-up cfd simulations by combining σ-y eulerian atomization model with a response surface methodology under diesel engine-like conditions (ecn spray a), Computers & Fluids 156 (2017) 9–20.

[40] S. B. Pope, Ten questions concerning the large-eddy simulation of turbulent flows, New journal of Physics 6 (1) (2004) 35.

[41] J. Fröhlich, C. P. Mellen, W. Rodi, L. Temmerman, M. A. Leschziner, Highly resolved large-eddy simulation of separated flow in a channel with streamwise periodic constrictions, Journal of Fluid Mechanics 526 (2005) 19–66.

[42] H. Werner, H. Wengle, Large-eddy simulation of turbulent flow over and around a cube in a plate channel, in: Turbulent Shear Flows 8, Springer, 1993, pp. 155–168.

[43] J. Roenby, H. Bredmose, H. Jasak, A computational method for sharp interface advection, Open Science 3 (11). doi:10.1098/rsos.160405.
URL http://rsos.royalsocietypublishing.org/content/3/11/160405

[44] F. Denner, D. R. van der Heul, G. T. Oud, M. M. Villar, A. da Silveira Neto, B. G. van Wachem, Comparative study of mass-conserving interface capturing frameworks for two-phase flows with surface tension, International Journal of Multiphase Flow 61 (2014) 37–47.

[45] A. Ferrari, M. Magnini, J. R. Thome, A flexible coupled level set and volume of fluid (flexclv) method to simulate microscale two-phase flow in non-uniform and unstructured meshes, International Journal of Multiphase Flow 91 (2017) 276–295.

[46] D. Fuster, A. Bagué, T. Boeck, L. Le Moyne, A. Leboissetier, S. Popinet, P. Ray, R. Scardovelli, S. Zaleski, Simulation of primary atomization with an octree adaptive mesh refinement and vof method, International Journal of Multiphase Flow 35 (6) (2009) 550–565.

[47] N. Hecht, Simulation aux grandes échelles des écoulements liquide-gaz : application á l'atomisation, Ph.D. thesis, University of Rouen (2014).

[48] B. Duret, J. Reveillon, T. Menard, F. Demoulin, Improving primary atomization modeling through dns of two-phase flows, International Journal of Multiphase Flow 55 (2013) 130–137.

[49] Engine Combustion Network, `https://ecn.sandia.gov/`.

[50] J. Desantes, J. García-Oliver, J. Pastor, A. Pandal, E. Baldwin, D. Schmidt, Coupled/decoupled spray simulation comparison of the ecn spray a condition with the σ-y eulerian atomization model, International Journal of Multiphase Flow 80 (2016) 89–99.

[51] J. M. Garcia-Oliver, J. M. Pastor, A. Pandal, N. Trask, E. Baldwin, D. P. Schmidt, Diesel spray cfd simulations based on the σ-y eulerian atomization model, Atomization and Sprays 23 (1) (2013) 71–95.

[52] J. Anez, A. Ahmed, S. Puggelli, J. Reveillon, J. C. Brändle de Motta, F.-X. Demoulin, Subgrid liquid flux and interface modelling for les of atomization,

in: Ilass Europe. 28th european conference on Liquid Atomization and Spray Systems, Editorial Universitat Politècnica de València, 2017, pp. 385–393.

[53] A. L. Kastengren, F. Z. Tilocco, C. F. Powell, J. Manin, L. M. Pickett, R. Payri, T. Bazyn, Engine combustion network (ecn): measurements of nozzle geometry and hydraulic behavior, Atomization and Sprays 22 (12) (2012) 1011–1052.

[54] S. B. Pope, Turbulent flows, IOP Publishing, 2001.

[55] J. Matheis, S. Hickel, Multi-component vapor-liquid equilibrium model for les of high-pressure fuel injection and application to ecn spray a, International Journal of Multiphase Flow 99 (2018) 294–311.

[56] E. Knudsen, E. Doran, V. Mittal, J. Meng, W. Spurlock, Compressible eulerian needle-to-target large eddy simulations of a diesel fuel injector, Proceedings of the Combustion Institute 36 (2) (2017) 2459–2466.

[57] G. Lacaze, A. Misdariis, A. Ruiz, J. C. Oefelein, Analysis of high-pressure diesel fuel injection processes using les with real-fluid thermodynamics and transport, Proceedings of the Combustion Institute 35 (2) (2015) 1603–1611.

[58] Engine combustion network | near-nozzle mixture derived from x-ray radiography.
URL `https://ecn.sandia.gov/rad675/`

[59] A. Kastengren, F. Tilocco, D. Duke, C. Powell, S. Moon, X. Zhang, Time-resolved x-ray radiography of diesel injectors from the engine combustion network, ICLASS Paper (2012) 1369.

[60] L. M. Pickett, J. Manin, A. Kastengren, C. Powell, Comparison of near-field structure and growth of a diesel spray using light-based optical microscopy and x-ray radiography, SAE International Journal of Engines 7 (2014-01-1412) (2014) 1044–1053.

[61] A. L. Kastengren, C. F. Powell, Y. Wang, K.-S. Im, J. Wang, X-ray radiography measurements of diesel spray structure at engine-like ambient density, Atomization and Sprays 19 (11) (2009) 1031–1044.

[62] R. Payri, S. Molina, F. Salvador, J. Gimeno, A study of the relation between nozzle geometry, internal flow and sprays characteristics in diesel fuel injection systems, KSME International Journal 18 (7) (2004) 1222–1235.

[63] R. Payri, B. Tormos, J. Gimeno, G. Bracho, The potential of large eddy simulation (les) code for the modeling of flow in diesel injectors, Mathematical and Computer Modelling 52 (7-8) (2010) 1151–1160.

[64] M. Sussman, E. G. Puckett, A coupled level set and volume-of-fluid method for computing 3d and axisymmetric incompressible two-phase flows, Journal of computational physics 162 (2) (2000) 301–337.

[65] L.-M. Malbec, J. Egúsquiza, G. Bruneaux, M. Meijer, Characterization of a set of ecn spray a injectors: nozzle to nozzle variations and effect on spray characteristics, SAE International Journal of Engines 6 (2013-24-0037) (2013) 1642–1660.